UNIVERSITY OF
COPENHAGEN

Myers–Perry Black Holes as Blackfolds

Sacha Perry-Fagant

Supervised by Jay Armas and Troels Harmark

Master's Thesis in Physics 2019/2020

Acknowledgements

First and foremost, I would like to thank my supervisor Jay Armas, for guiding me through my thesis, patiently answering all my questions and imparting much knowledge to me. Secondly, a huge thank you to my co-supervisor Troels Harmark for his dedication in finding me a good thesis and his help throughout. I would like to mention my appreciation for the Niel's Bohr Institute for giving me the opportunity to pursue this degree.

Thank you to my family for showing interest in my thesis and for all their support. A big thank you to my mother for her help editing and for her physics jokes.

Thank you to Ivan, Mariana and Dani for help with my thesis, late night talks about conformal transformations and making the whole process a little easier.

A special thanks to Dani for dealing with my dramatics, easing my doubts and always being there when I needed him.

Nothing in life is to be feared, it is only to be understood. Now is the time to understand more, so that we may fear less.
— Marie Curie

Abstract

Black holes in dimensions > 4 can take on new properties and topologies compared to those in 4 dimensions. We examine the Myers–Perry black hole, a rotating black hole in $D > 4$ dimensions and take it to the ultra-spinning limit. In this limit, where the horizon exhibits two widely separated length scales, we explicitly show that Myers–Perry black holes are described by the blackfold effective theory up to first order in a derivative expansion. We conjecture that the second order blackfold approximation of Myers–Perry black holes can be obtained by applying the fluid/gravity correspondence. Using results obtained in this manner, we examine the expected higher order metrics and associated energy-momentum tensors. We review the comparison of the Gregory–Laflamme instability to hydrodynamic perturbations.

Contents

1 Introduction

As far as we can tell with our senses, we live our everyday lives in four dimensions. We move as we please through space, and perhaps not *quite* as we please through time. Without physics, we might never have seriously considered that this four-dimensional assumption could be wrong. Physicists have been able to learn much about the universe while assuming four dimensions, but jumped at the chance of incorporating more. With the allowance of additional dimensions came more ideas, theories and solutions. A good example of this is string theory; bosonic string theory requires 26 dimensions, M-theory requires 11 and superstring theory requires 10. Another example is Kaluza-Klein theory, which attempts to create a unified theory by adding a compactified 5^{th} dimension.

Even if we find that our universe is simply comprised of four dimensions, studying higher dimensional regimes will not be for naught. In studying these higher dimensional regimes, we can probe certain cases that we cannot in four dimensions. For example, the Gregory–Laflamme instability is an instability that affects thin black branes and strings via perturbations of the thickness. One of the possible endpoints of the instability results in naked singularities and studying this case could reveal more about the nature of black holes in general. Another example is the fluid/gravity correspondence which, as the names suggests, relates fluid dynamics to gravitational dynamics, allowing one to map solutions on one side to the other side. In this way, we can gain insight into fluid dynamics given gravitational solutions.

However, with more dimensions comes more complexity. For instance, vacuum black holes in four dimensions can be described by two parameters: mass and angular momentum. In higher dimensions there are more conserved charges and specifying these charges is not always enough to know what the solution is. When $D = 4$, there is only one solution for neutral black holes: the Kerr solution, in which the Schwarzschild solution is obtained in the static case. The more dimensions we have, the more new black hole topologies exist, along with the possibility to rotate in more planes. However, finding solutions that satisfy Einstein's equations in higher dimensions is not simple. Physicists have tasked themselves both with finding solutions as well as developing techniques to simplify calculations. This is where the blackfold approach comes in. The

blackfold approach allows one to perturbatively fold black brane solutions possessing two widely differing length scales into different shapes, for example, constructing a black ring from a black string. The blackfold approach is a long wavelength effective theory; in this case, this means that the brane varies on scales much larger than its thickness.

Another application of the blackfold approach is to the Myers–Perry black hole, a spinning spherical black hole in higher dimensions, which serves as the main focus of this thesis. The blackfold approach can be applied to the Myers–Perry black hole in the ultra-spinning regime, in which the black hole pancakes out into a disk shape. The blackfold approach consists of finding an overlap region of solutions far and near the horizon of the black hole, and once it has been applied, we can examine some properties of the black hole, most notably the energy-momentum tensor. It has been shown previously that in the overlap region, at ideal order, the energy-momentum tensor is that of a perfect fluid. Our thesis consists of verifying these results and investigating the effect of higher order corrections on the metric and the energy-momentum tensor.

We start off in section 2 by giving a summary of relevant General Relativity (GR) formulas and conventions, then in section 3, we explain the changes to GR in higher dimensions and discuss some new black hole solutions that arise. In section 4 we go over the blackfold approach and in section 5 we review two methods of finding the energy-momentum tensor: linearized gravity and the method of Brown and York. We give a review of the important concepts of the fluid/gravity correspondence in section 6. In section 7, we apply the blackfold approach to the ultra-spinning Myers–Perry black hole, starting by verifying the energy-momentum tensor for the ideal order case. Next, in section 7.2, we compute the first order metric and compare our results to work done in [1] and [2] giving a brief summary of the papers, where hydrodynamic perturbations are applied to black holes. We then review the work done in [3], where second order perturbed black holes are constructed by applying the previously mentioned fluid/gravity correspondence along with the AdS/Ricci-flat correspondence, which maps asymptotically AdS solutions to asymptotically Ricci-flat solutions. We review the instability and comment on the results when applied to the parameters of the Myers–Perry metric. We review the Gregory–Laflamme instability in section 8 and compare it to hydrodynamic perturbations. We end in section 9 with a summary of the results and important points of this thesis, and mention possible future work.

2 Conventions and Prerequisites

In this section we go over the basic conventions and notation necessary to follow this thesis. While it is assumed that the reader has an understanding of general relativity, we start off by giving an overview of the required GR formulas used throughout this thesis. We end by listing our conventions.

2.1 General Relativity Formulas

In this section we present the basic formulas in general relativity needed to carry out our calculations. We do not go into detail as it is assumed that the reader is familiar with these concepts, and if not, we refer them to [4]. General relativity is a way of understanding the geometry of spacetime and the objects that can affect it. It allows us to study cosmology, gravitational waves and, most importantly for this thesis, black holes.

2.1.1 Basic Formulas

In order to study physics in any framework, one of the key tools one must have is the ability to take derivatives. Taking derivatives in a curved space is not as straight forward as in a flat space, as we must take into account how the quantity changes from point to point on curves of spacetime. The laws of physics obey the principle of general covariance, which states that they do not change under coordinate transformations. In order to abide by this rule in curved spaces, a covariant derivative is required. The covariant derivative of a one-form A_ν and vector V^ν is defined as:

$$\begin{aligned} \nabla_\mu A_\nu &= \partial_\mu A_\nu - \Gamma^\lambda_{\mu\nu} A_\lambda, \\ \nabla_\mu V^\nu &= \partial_\mu V^\nu + \Gamma^\nu_{\mu\lambda} V^\lambda, \end{aligned} \tag{2.1}$$

where $\Gamma^{\lambda}_{\mu\nu}$ are the Christoffel symbols

$$\Gamma^{\lambda}_{\mu\nu} = \frac{1}{2} g^{\lambda\sigma} \left(\partial_\mu g_{\nu\sigma} + \partial_\nu g_{\mu\sigma} - \partial_\sigma g_{\mu\nu} \right), \tag{2.2}$$

and for a general tensor $T^{\mu_1 \cdots \mu_n}_{\nu_1 \ldots \nu_m}$, the covariant derivative is

$$\begin{aligned} \nabla_\sigma T^{\mu_1 \ldots \mu_n}_{\nu_1 \ldots \nu_m} = \partial_\sigma T^{\mu_1 \ldots \mu_n}_{\nu_1 \ldots \nu_m} \\ + \Gamma^{\mu_1}_{\lambda\sigma} T^{\lambda \ldots \mu_n}_{\nu_1 \ldots \nu_m} + \ldots + \Gamma^{\mu_n}_{\lambda\sigma} T^{\lambda \ldots \lambda}_{\nu_1 \ldots \nu_m} \\ - \Gamma^{\lambda}_{\nu_1\sigma} T^{\mu_1 \ldots \mu_n}_{\lambda \ldots \nu_m} - \ldots - \Gamma^{\lambda}_{\nu_m\sigma} T^{\mu_1 \ldots \mu_n}_{\nu_1 \ldots \lambda}. \end{aligned} \tag{2.3}$$

Here, $g_{\mu\nu}$ signifies the background spacetime metric, but the covariant derivative can also be defined in a subspace, or on a manifold. Using the covariant derivative, we can probe the curvature of the spacetime, or manifold, to find the Riemann curvature tensor:

$$R^{\mu}_{\ \nu\rho\sigma} = \partial_\rho \Gamma^{\mu}_{\nu\sigma} - \partial_\sigma \Gamma^{\mu}_{\nu\rho} + \Gamma^{\mu}_{\alpha\rho} \Gamma^{\alpha}_{\nu\sigma} - \Gamma^{\mu}_{\alpha\sigma} \Gamma^{\alpha}_{\nu\rho}. \tag{2.4}$$

This tensor can be used to tell whether or not a spacetime is flat, in which case $R^{\mu}_{\ \nu\rho\sigma} = 0$. From this, we get the Ricci tensor, $R_{\mu\nu}$ and scalar, R, by contracting with the metric $g_{\mu\nu}$

$$\begin{aligned} R_{\mu\nu} &= R^{\rho}_{\ \mu\rho\nu} = g^{\rho\sigma} g_{\alpha\sigma} R^{\alpha}_{\ \mu\rho\nu}, \\ R &= R^{\mu}_{\mu} = g^{\mu\nu} R_{\mu\nu}, \end{aligned} \tag{2.5}$$

which, again, are zero in flat space. With this, we can now define Einstein's equations[1]:

$$R_{\mu\nu} - \frac{1}{2} R g_{\mu\nu} = 8\pi T_{\mu\nu}, \tag{2.6}$$

where $T_{\mu\nu}$ is the energy-momentum (or stress-energy) tensor. We go into more detail about the energy-momentum tensor in section 5. We can also find these equations through the variation of the Einstein-Hilbert action:

$$I = \frac{1}{16\pi} \int d^D x \sqrt{-g} R. \tag{2.7}$$

[1] In this thesis, unless otherwise specified, we assume $\Lambda = 0$.

2.1.2 Submanifolds

Rather than looking at the entire spacetime backgroumd, we can focus on a submanifold, embedded in the spacetime. We define a map from the background spacetime onto the subspace, $X^\mu(\sigma)$, which can then be used to find the induced metric on the submanifold [5]:

$$\gamma_{ab} = g_{\mu\nu}\partial_a X^\mu \partial_b X^\nu, \tag{2.8}$$

where we used the pullback map $\partial_a X^\mu$, which allows us to map background tensors to worldvolume tensors and vice versa. For example, if we have a spacetime metric [6]

$$ds^2 = -dt^2 + d\rho_1^2 + \rho_1^2 d\phi_1^2 + d\rho_2^2 + \rho_2^2 d\phi_2^2 + \delta_{ij}dx^i dx^j, \tag{2.9}$$

with i, j ranging in $(1, n)$, and embedding

$$\begin{aligned} &X^t = t, \qquad X^{\rho_1} = \rho_1, \qquad X^{\phi_1} = \phi_1, \\ &X^{\rho_2} = 0, \qquad X^{\phi_2} = 0, \qquad X^{x_i} = 0, \end{aligned} \tag{2.10}$$

we get the induced metric

$$\gamma_{ab} = -dt^2 + d\rho_1^2 + \rho_1^2 d\phi_1^2. \tag{2.11}$$

As one can see, there are fewer dimensions on the submanifold compared to the background spacetime. We denote this subset of coordinates as *worldvolume coordinates*. A worldvolume is the volume that the subspace takes up, including the time direction. An easy to visualize example of this is given by string theory, where a string carves out a two-dimensional worldsheet, fig. 1. From the embedding map, we can find the first fundamental tensor

$$h^{\mu\nu} = \gamma^{ab}\partial_a X^\mu \partial_b X^\nu, \tag{2.12}$$

which acts as a projector onto the worldvolume. One can also find

$$\perp_{\mu\nu} = g_{\mu\nu} - h_{\mu\nu}, \tag{2.13}$$

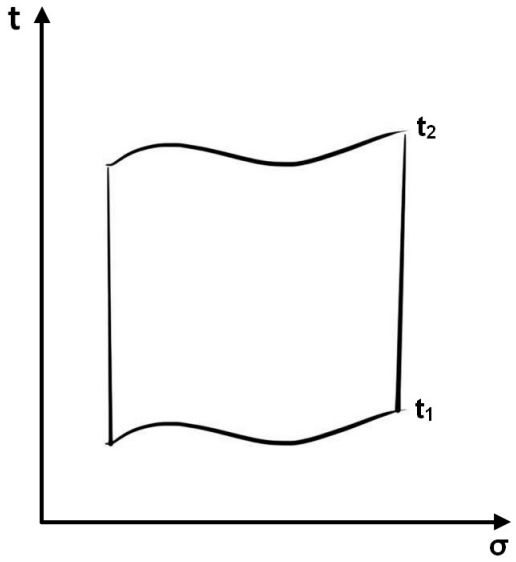

Figure 1: A string evolving from time t_1 to t_2, with σ representing the space coordinate, creating a 2-dimensional worldsheet.

which projects along directions orthogonal to the worldvolume. $h_{\mu\nu}$ can then be used to find the extrinsic curvature $K^{\rho}_{\mu\nu}$, which is the curvature of a submanifold caused by the embedding. The background spacetime does not have an extrinsic curvature, as we typically assume that the spacetime is not embedded in a higher dimensional space. We go into more detail on how $K^{\rho}_{\mu\nu}$ is derived in section 5.2.

2.1.3 Derivation of D=4 Schwarzschild Metric

Calculations are often much simpler in 4 dimensions. This fact is exemplified by the straightforward derivation of the Schwarzschild metric in 4 dimensions. Here, we will give a brief derivation of this metric, following the procedure of [7]. One can start by looking at the background spacetime Minkowski metric

$$ds^2 = -dt^2 + dr^2 + r^2 d\omega^2 + r^2 \sin^2 \omega d\omega_2^2. \tag{2.14}$$

A solution in this background will have the general form of

$$ds^2 = -Udt^2 + Vdr^2 + Wr^2 d\omega^2 + Xr^2 \sin^2\omega d\omega_2^2, \tag{2.15}$$

where U, V, W and X are functions that must be solved for. We are looking for a metric that obeys the following constraints

- Static: $\partial_t g_{\mu\nu} = 0$,
- Spherically symmetric,
- Obeys vacuum Einstein equations: $R_{\mu\nu} - \frac{1}{2} g_{\mu\nu} R = 0$.

The first requirement demands that the functions do not depend on t explicitly, and the second that they do not depend on ω or ω_2. In addition, the second requirement allows one to set $V = W = 1$. In all, the functions become

$$U \to U(r), \qquad V \to V(r), \qquad W \to 1, \qquad V \to 1. \tag{2.16}$$

The last constraint is satisfied by first finding the Christoffel symbols $\Gamma^{\lambda}_{\mu\nu}$ using (2.2), and then finding the Riemann curvature tensor, using (2.4), which is used to find $R_{\mu\nu}$ and R. The third constraint is then used to solve for $U(r)$ and $V(r)$ which turn out to be

$$U = \left(1 - \frac{C}{r}\right), \qquad V = \frac{1}{\left(1 - \frac{C}{r}\right)}. \tag{2.17}$$

Using the fact that the background metric should be recovered as $r \to \infty$ as well as when the mass $M \to 0$, C is found to be

$$C = 2M, \tag{2.18}$$

which we typically set as r_s, the radius of the event horizon.

2.2 Conventions and Notation

In reading the previous sections, one may have picked up on some of the conventions used in this thesis but we make our conventions explicit in this section.
The gravitational constant G = 1.
The speed of light c = 1.
The indices (a, b) signify worldvolume coordinates while (μ, ν) signify the background spacetime coordinates. For example, we denote the background spacetime by $g_{\mu\nu}$ and the induced metric on the manifold as γ_{ab}. The first fundamental tensor, $h_{\mu\nu}$, is raised and lowered with the background spacetime metric. The total dimension of the spacetime is $D = p+n+3$, p being the number of spatial worldvolume coordinates, plus one for time, and $n+2$ transverse directions. Quantities with (a, b) range over $p+1$, while (μ, ν) range over D. The covariant derivative on the background spacetime is ∇_μ and D_a is for the worldvolume metric. Occasionally we will use d rather than D to denote the spacetime dimension so as not to get confused with the covariant derivative D_a. The Ω_{n+1} coordinates are expressed with ω_i, not to be confused with θ which, when used as a coordinate, is one of the worldvolume coordinates. For example, for n=2 we would have

$$d\Omega_3^2 = d\omega_1^2 + \sin^2\omega_1 d\omega_2^2 + \sin^2\omega_1 \sin^2\omega_2 d\omega_3^2. \tag{2.19}$$

We denote the radius of the brane as r_+, if brane has several radii, r_+ is the smaller radius and $r_o = r_+ \cos\theta$ is what is called the thickness.

3 Black holes in Higher Dimensions

When considering the existence of more dimensions, one might wonder how these dimensions could exist when we do not measure them. There are two main explanations for this issue [8]. One posits that the higher dimensions could be so small, and periodic, such that we do not measure them, meaning these dimensions are compactified. The other supposes that four-dimensional spacetime as we know it, is simply a subspace embedded in a higher dimensional space with the fields in the standard model confined to it. One might also wonder how the laws of physics change when going into higher dimensions. In this section we will give an overview of some of the differences when doing calculations in GR in higher dimensions. We also discuss some of the new solutions one can get in higher dimensions, Myers–Perry black holes in section 3.2 and black rings in section 3.3. This section serves more or less as a partial review of [9].

3.1 General Relativity in $D > 4$

In some ways, four-dimensional black holes are quite limited compared to those in higher dimensions. For example, they are limited to a spherical topology, which is not the case in higher dimensions. In four dimensions, a black hole can only possess one independent angular momentum, given that it can rotate in the (x, y)-plane, (x, z)-plane or (y, z)-plane. In general, they can rotate in up to $\lfloor \frac{D-1}{2} \rfloor$ independent planes, again we achieve this number of planes by taking pairs of spatial dimensions (x_i, x_j), each with an associated angular momentum J_i. In higher dimensions, the relation between the gravitational potential,

$$V_g = -\frac{M}{r^{d-3}}, \tag{3.1}$$

and centrifugal barrier,

$$V_c = \frac{J^2}{M^2 r^2}, \tag{3.2}$$

changes, as gravitational potential depends on the dimension and the centrifugal barrier does not. As the number of dimensions increase, the gravitational potential weakens thus the centrifugal force required to counterbalance the gravitational attraction de-

creases.

In four dimensions, there is the famous "no-hair" theorem that states that a black hole can be completely characterized by its mass, charge and angular momentum, these solutions being given by the Kerr-Newman family of solutions [8]. In higher dimensions, there is no analogue, in the way that a unique solution cannot be found only from conserved charges. It is still possible that a uniqueness theorem can be found in certain cases with the addition of some other parameters, but there is no guarantee. Black holes in four dimensions also have the rigidity theorem that states that stationary black holes must either be static or axisymmetric around the plane of rotation [10]. In higher dimensions, the black hole must only be symmetric along one axis of rotation [11]. A good example of this is the black ring, which is symmetric in the plane in which it must rotate to avoid gravitational collapse. These theorems, among others related to black hole uniqueness, are reviewed in more detail in [8]. Interesting to note is that the Bekenstein-Hawking entropy does not change in higher dimensions and is always

$$S = \frac{A_H}{4}, \tag{3.3}$$

where A_H is the area of the event horizon. As for black holes themselves, in four dimensions, there is one solution for the metric of an uncharged black hole. For static black holes, it turns into the Schwarzschild solution

$$ds^2 = -\left(1 - \frac{r_o}{r}\right) dt^2 + \frac{dr^2}{1 - \frac{r_o}{r}} + r^2 d\omega_1^2 + r^2 \sin^2 \omega_1 d\omega_2^2, \tag{3.4}$$

and the Kerr solution for rotating black holes

$$\begin{aligned} ds^2 = & -\left(1 - \frac{r_o r}{\Sigma}\right) dt^2 - \frac{2ar_o r}{\Sigma} \sin^2\theta dt d\phi \\ & + \frac{\left(r^2 + a^2\right)^2 - \Delta a^2 \sin^2\theta}{\Sigma} \sin^2\theta d\phi^2 + \frac{\Sigma}{\Delta} dr^2 + \Sigma d\theta^2, \\ \Sigma = r^2 + a^2 \cos^2\theta, & \qquad \Delta = r^2 - r_o r + a^2. \end{aligned} \tag{3.5}$$

In higher dimensions, the Schwarzschild solution does not undergo a big change and is

now of the form [9]

$$ds^2 = -\left(1 - \frac{\mu}{r^n}\right) dt^2 + \frac{dr^2}{1 - \frac{\mu}{r^n}} + r^2 d\Omega_{n+1}^2, \tag{3.6}$$

where $\mu = \frac{16\pi M}{(n+1)\Omega_{n+1}}$ is the mass parameter. The analogue of the Kerr solution is not as simple and we discuss it in the next section.

3.2 Myers–Perry Black Holes

For rotating black holes in dimension $D > 4$, we have Myers–Perry black holes, which serve as the main focus of this thesis. We are specifically interested in the $D \geq 6$ case, we will discuss why shortly. For a singly-spinning Myers–Perry black hole in $n + 5$ dimensions, the metric is [6]

$$\begin{aligned} ds^2 = & -dt^2 + \frac{\mu}{r^n \Sigma}(dt - a\sin^2\theta d\phi)^2 + \frac{\Sigma}{\Delta} dr^2 + \Sigma d\theta^2 + (r^2 + a^2)\sin^2\theta d\phi^2 \\ & + r^2 \cos^2\theta d\Omega_{n+1}^2, \end{aligned} \tag{3.7}$$

where

$$\Sigma = r^2 + a^2\cos^2\theta, \qquad \Delta = r^2 + a^2 - \frac{\mu}{r^n}, \tag{3.8}$$

and for doubly-spinning (possessing two angular momenta)

$$\begin{aligned} ds^2 = & -dt^2 + \sum_{i=1}^{2}[a_i^2 d\mu_i^2 + (r^2 + a_i^2)\mu_i^2 d\phi_i^2] + \frac{\mu}{r^{n+2}\Pi F}(dt - \sum_{i=1}^{2} a_i \mu_i^2 d\phi_i)^2 \\ & + \frac{\Pi F}{\Pi - \frac{\mu}{r^{n+2}}} dr^2 + r^2[d\theta^2 + \cos^2\theta(d\psi^2 + \cos^2\psi d\Omega_{(n-1)}^2)], \end{aligned} \tag{3.9}$$

where

$$\mu_1 = \sin\theta, \qquad \mu_2 = \cos\theta\sin\psi, \tag{3.10}$$

$$\Pi = \prod_{i=1}^{2}(1 + \frac{a_i^2}{r^2}), \qquad F = 1 - \sum_{i=1}^{2} \frac{a_i^2 \mu_i^2}{r^2 + a_i^2}. \tag{3.11}$$

In the singly-spinning case, the mass and angular momentum are

$$M = \frac{(d-2)\Omega_{n+3}}{16\pi}\mu, \qquad J = \frac{2}{n+3}Ma, \tag{3.12}$$

and the a_i's are approximately the angular momentum per unit mass. An interesting feature to take note of is the relationship between gravitational attraction and centrifugal repulsion. In order for them to be balanced we must have the equality

$$\frac{\Delta}{r^2} - 1 = -\frac{\mu}{r^{d-3}} + \frac{a^2}{r^2}. \tag{3.13}$$

The gravitational attraction, roughly equal to the first term on the right (as μ is related to mass via the equation above), depends on the number of dimensions and becomes weaker as n increases, while the second term, the repulsion term $\frac{a^2}{r^2}$, does not. Interestingly, the gravity term becomes smaller, requiring less centrifugal repulsion as n increases.

The general solution takes on a slightly different form depending on whether D is even or odd. When D is odd the solution is [9]

$$ds^2 = -dt^2 + (r^2 + a_i^2)(d\mu_i^2 + \mu_i^2 d\phi_i^2) + \frac{\mu r^2}{\Pi F}\left(dt - a_i\mu_i^2 d\phi_i\right)^2 + \frac{\Pi F}{\Pi - \mu r^2}dr^2, \tag{3.14}$$

and when D is even it is

$$ds^2 = -dt^2 + r^2 d\alpha^2 + (r^2 + a_i^2)(d\mu_i^2 + \mu_i^2 d\phi_i^2) + \frac{\mu r}{\Pi F}\left(dt - a_i\mu_i^2 d\phi_i\right)^2 + \frac{\Pi F}{\Pi - \mu r}dr^2, \tag{3.15}$$

where $\mu_i^2 + \alpha = 1$ and

$$F(r, \mu_i) = 1 - \frac{a_i^2\mu_i^2}{r^2 + a_i^2}, \qquad \Pi(r) = \prod_{i=1}^{N}(r^2 + a_i^2). \tag{3.16}$$

The event horizon is found by taking the largest real root of g^{rr}

$$\Pi(r_o) - \mu r_o^{\mathfrak{p}} = 0, \tag{3.17}$$

where $\mathfrak{p} = 2$ in the odd case and $\mathfrak{p} = 1$ in the even case.

The Myers–Perry black hole may not appear new and exciting at first glance as it is similar to the four-dimensional Kerr metric, especially in the singly-spinning case as it is again a spherical rotating black hole. However, unlike Kerr, with large angular momenta the Myers–Perry black hole can become extended in $D > 5$, allowing one to explore more solutions and phenomena. To see why we cannot have this phenomenon in $D = 5$, we take the example of the singly-spinning case where for $D = 5$, the largest real positive root of Δ is $r_o = \sqrt{\mu - a^2}$. This provides a limit on a, requiring $a < \sqrt{\mu}$. Note that in the $a = \sqrt{\mu}$ case there would be a naked singularity as $r_o = 0$. This issue is not present in $D \geq 6$, allowing a to be arbitrarily large. This will be discussed further in section 7.

3.3 Black Rings

In $D = 5$, black rings have topology $S^1 \times S^2$, where we let S^2 be the smaller ring thickness, and S^1 be the larger overall ring with topology maintained by the centrifugal force of the rotation[2]. The solution of a black ring with one angular momentum is [9]

$$\begin{aligned} ds^2 = &- \frac{F(y)}{F(x)}\left(dt - CR\frac{1+y}{F(y)}d\psi\right)^2 \\ &+ \frac{R^2}{(x-y)^2}F(x)\left(-\frac{G(y)}{F(y)}d\psi^2 - \frac{dy^2}{G(y)} + \frac{dx^2}{G(x)} + \frac{G(x)}{F(x)}d\phi^2\right), \end{aligned} \tag{3.18}$$

where

$$\begin{aligned} F(z) = 1 + \lambda z, \qquad G(z) = (1-z^2)(1+\nu z), \\ C = \sqrt{\lambda(\lambda-\nu)\frac{1+\lambda}{1-\lambda}}, \end{aligned} \tag{3.19}$$

[2]Setting S^1 as the smaller radius and S^2 as the larger radius is also valid.

and R is the larger radius, and λ and ν are dimensionless parameters in the range $0 < \nu \leq \lambda < 1$. The range of x and y are

$$\begin{aligned} -1 \leq x \leq 1, \\ -\infty \leq y \leq -1, \end{aligned} \tag{3.20}$$

with asymptotic infinity at $x \to y \to -1$. The rotation is around ψ at $y = -1$. In order to avoid a conical defect, the angular values must have periodicity

$$\Delta\psi = \Delta\phi = 4\pi \frac{\sqrt{F(-1)}}{|G'(-1)|} = 2\pi \frac{\sqrt{1-\lambda}}{1-\nu}, \tag{3.21}$$

and λ and ν must obey

$$\lambda = \frac{2\nu}{1+\nu^2}. \tag{3.22}$$

These constraints allow for the ring solutions to be characterized by (ν, R). One can think of ν as the ratio between S^2 and S^1.

If one does not eliminate λ through (3.22), then the Myers–Perry black hole can be recovered as a limit of the black ring [12] by taking $R \to 0$, $\lambda \to 1$, and $\nu \to 1$, and defining fixed parameters a and m

$$m = \frac{2R^2}{1-\nu}, \qquad a^2 = 2R^2 \frac{\lambda - \nu}{(1-\nu)^2}, \tag{3.23}$$

then making the change of coordinates from (x, y) to (r, θ)

$$x = -1 + 2\left(1 - \frac{a^2}{m}\right) \frac{R^2 \cos^2\theta}{r^2 - (m-a^2)\cos^2\theta}, \tag{3.24}$$

$$y = -1 - 2\left(1 - \frac{a^2}{m}\right) \frac{R^2 \sin^2\theta}{r^2 - (m-a^2)\cos^2\theta}, \tag{3.25}$$

and rescaling $(\psi, \phi) \to \sqrt{\frac{m-a^2}{2R^2}}(\psi, \phi)$ gives a solution in the form of (3.7), when $n = 0$.

One can look at the phase space of the ring by examining the dimensionless param-

eters a_H, the horizon area, and spin j

$$a_H = 2\sqrt{\nu(1-\nu)}, \qquad j = \sqrt{\frac{(1+\nu)^3}{8\nu}}. \tag{3.26}$$

Because one can write a_H in terms of j, we put our discussion in terms of j. There are three possible solutions depending on these values: thin rings (with small S^2 compared to S^1), fat rings and Myers–Perry black holes. In the range $\sqrt{27/32} \leq j \leq 1$, all three of these solutions exist for the same j. This confirms our earlier statement about how higher dimensional black holes are non-unique.

We obtain a second angular momentum by letting S^2 rotate. In the limit where S^2 is infinitely big, each S^2 segment along the ring can be thought of as a four-dimensional rotating black hole. The solution can be written as:

$$\begin{aligned} ds^2 = & -\frac{H(y,x)}{H(x,y)}(dt+\Omega)^2 - \frac{F(x,y)}{H(y,x)}d\psi^2 - 2\frac{J(x,y)}{H(y,x)}d\psi d\phi + \frac{F(y,x)}{H(y,x)}d\phi^2 \\ & - \frac{2k^2 H(x,y)}{(x-y)^2(1-\nu)^2}\left(\frac{dx^2}{G(x)} - \frac{dy^2}{G(y)}\right), \end{aligned} \tag{3.27}$$

where ϕ and ψ now have period 2π, and k tells us about the scale and can be thought of as roughly the radius. The form of the functions in the metric in general are quite complex but are much simpler when the forces are balanced and there are no conical singularities. The form of the functions in this case are given in (F.1). Again, the doubly-spinning Myers–Perry black hole can be recovered from a limit of the solution, but only in the general case. In terms of the angular momenta J_ϕ and J_ψ one can define j_ϕ and j_ψ as in the previous case, and the phase space can be examined. There are three regions of phase space for specific j_i values. Maximum J_ϕ for the given J_ψ gives extremal black rings, minimum J_ψ for the given J_ϕ gives non-extremal minimally spinning black rings, and otherwise limiting extremal Myers–Perry black holes. There is again a range of j_i values for which all three solutions exist. An interesting note about black ring temperature is that when the ring becomes infinitely long and thin, and J_ϕ is taken to the extremal limit, the temperature goes to zero.

Black rings are a good illustrative example of general relativity in $D > 4$, as they provide a new brane topology not seen in $D = 4$, as well as demonstrate the non-

uniqueness of $D > 4$ solutions.

4 Blackfold Approach

The definition of a blackfold is "a black p-brane whose worldvolume extends along a curved submanifold of the embedding spacetime" [13]. The blackfold approach is an effective worldvolume theory for the dynamics of black branes, applicable when the black hole has differing length scales. This technique does not typically apply in four dimensions as the length scales are of similar order. Higher dimensional black holes have more possibilities for differing scales for example, neutral black holes can have wildly differing mass and angular momentum. Black rings also fall into this category as they have two radii, one of which can be much smaller than the other.

4.1 Procedure

Blackfolds allow us to investigate certain solutions by using a *probe* brane, which is a simpler version of the original solution, by making use of the differing scales. For example, in the ultra-spinning limit of a black hole, the black hole becomes very thin and wide. In this case, the differing scales are the smaller radius $s = r_o$ and the larger radius $S = R$, and the solution is taken to first order in $\frac{r_o}{R}$. At ideal order, we ignore back-reactions of the brane on the background geometry.

The blackfold approach consists of examining the metric in three regions:

1. $r \ll S$
2. $r \gg s$
3. $s \ll r \ll S$.

The solution in the overlap region 3 is found through the other two regions. Finding solutions in this way is an example of a matched asymptotic expansion (MAE). MAEs are applicable when one encounters a problem for which different solutions can be found in different coordinate patches; the solutions in the different patches are then combined

to find a global solution. In general, solutions found in each region provide the other regions with boundary conditions.

In [14] this procedure is applied to find approximate solutions for black rings to first order. The zeroth order starting point is an infinitely long straight string, close to the horizon. The ideal order (boosted) Schwarzschild black string is

$$\begin{aligned} ds^2 =& \frac{dr^2}{1-\frac{r_o^n}{r^n}} + r^2\left(d\theta^2 + \sin^2\theta d\Omega_n^2\right) - \left(1-\frac{r_o^n}{r^n}\right)\left(\cosh\alpha dt + \sinh\alpha dz\right)^2 \\ &+ \left(\cosh\alpha dz + \sinh\alpha dt\right)^2 . \end{aligned} \tag{4.1}$$

A small curvature is then added to the string to find the first order correction. The asymptotic limit gives the solution of a string. To find the solution in the near region, one must find boundary conditions, which is done by matching the far and near solutions in the overlap zone. The near zone first order solution can then be used to find second order solutions. The MAE can then be continued using second order solutions to provide conditions for third order solutions, and so on and so forth. In Appendix E, we show the MAE calculations for singly and doubly-spinning Myers–Perry black holes.

This thesis deals with ultra-spinning black holes in higher dimensions. Taking one such metric and examining it in the region, $r \ll S$, one finds that, locally at each point, the metric describing the black hole is that of a boosted black brane [9]

$$ds^2 = \left(\gamma_{ab} + \frac{r_o^n}{r^n}u_a u_b\right) d\sigma^a d\sigma^b + \frac{dr^2}{1-\frac{r_o^n}{r^n}} + r^2 d\Omega^2_{(n+1)}, \tag{4.2}$$

where u_a corresponds to the boost velocities and γ_{ab} is the induced metric with (a, b) indices ranging from 0 to p. For example, it has been shown in [6] that taking a doubly-spinning Myers–Perry black hole, and applying the ultra-spinning limit to one of the angular momenta, results in a boosted singly-spinning MP black brane. Applying the ultra-spinning limit to a singly-spinning MP black hole produces a boosted Schwarzschild membrane. This technique, being a long-wavelength effective theory, requires for the velocities u_a, the transverse velocities $\partial X^\perp$, and r_o to vary slowly over the worldvolume [5], meaning they vary on scales $R \gg r_o$.

4.2 Blackfold Equations

In order to have a blackfold, certain conditions must be satisfied. For the source to be coupled to gravity, we must have [13]

$$\bar{\nabla}_\mu T_{\mu\nu} = 0, \tag{4.3}$$

where

$$\bar{\nabla}_\mu = h^\nu_\mu \nabla_\nu, \tag{4.4}$$

and $h_{\mu\nu}$ is the first fundamental tensor, which acts as a projector onto the worldvolume. The covariant derivative is written in this way because it is only well defined along tangential directions to the worldvolume. These equations can be split up into $D - p - 1$ extrinsic and $p + 1$ intrinsic equations by projecting along directions parallel and orthogonal to the worldvolume [15]

$$\begin{aligned} T^{\mu\nu} K^\rho_{\mu\nu} &= 0 \qquad \text{(extrinsic)}, \\ D_a T^{ab} &= 0 \qquad \text{(intrinsic)}, \end{aligned} \tag{4.5}$$

where D_a is the covariant derivative on the worldvolume and $K^\rho_{\mu\nu}$ is the extrinsic curvature. The extrinsic equation can be thought of as the analogue of (mass $\times$ acceleration $= 0$) to extended relativistic objects, and the intrinsic equations means that the tensor is conserved on the worldvolume. In the overlap region, assuming the worldvolume is isotropic [5], the stress-energy tensor is that of a perfect fluid:

$$T^{ab} = (\varepsilon + P)\, u^a u^b + P \gamma^{ab}, \tag{4.6}$$

$$\varepsilon = -(n+1)P = (n+1)\frac{\Omega_{n+1} r_o^n}{16\pi}, \tag{4.7}$$

where ε is the energy density, P is the pressure and Ω is the solid angle, given by [16]

$$\Omega_d = \frac{2\pi^{\frac{d+1}{2}}}{\Gamma(\frac{d+1}{2})}. \tag{4.8}$$

The associated velocities of this tensor also have the property $u_a \gamma^{ab} u_b = -1$. We can also rewrite the tensor as

$$T^{ab} = \frac{1}{16\pi} r_o^n \Omega_{(n+1)} n \left(u^a u^b - \frac{1}{n} \gamma^{ab} \right). \tag{4.9}$$

In this thesis, we focus on neutral black branes so we take this case and apply (4.3) to the perfect fluid tensor (4.9), the necessary equation becomes

$$\dot{u}^\mu + \frac{1}{n+1} u^\mu \bar{\nabla}_\nu u^\nu = \frac{1}{n} K^\mu + \bar{\nabla}^\mu \ln r_o, \tag{4.10}$$

where $\dot{u}^\mu = u^\nu \nabla_\nu u^\mu$ is the acceleration of u^μ. Again, these can be projected parallel and orthogonal to the worldvolume

$$K^\rho = n \perp^\rho_\mu \dot{u}^\mu, \tag{4.11}$$

$$\dot{u}_a + \frac{1}{n+1} u_a D_b u^b = \partial_a \ln r_o, \tag{4.12}$$

where $\dot{u}^b = u^c D_c u^b$. These are the *blackfold equations* which describe the dynamics of a neutral black brane, up to leading order [5].

5 Energy-Momentum Tensor of Branes

The energy-momentum tensor, also known as the stress-energy-momentum tensor, is a symmetric tensor that reveals a lot about a system, summarized by [17]:

T^{00}: Energy density

T^{i0}: Density of i$^{\text{th}}$ component of momentum

T^{0j}: Energy flux in i$^{\text{th}}$ direction

T^{ij}: Flux in j direction of i$^{\text{th}}$ momentum component.

This section describes two popular methods of finding the energy-momentum tensor in GR: linearized gravity and the method of Brown and York.

5.1 Linearized Gravity

The first method we look at is linearized gravity and we follow the notes of [18]. While in this section we use it to find the energy-momentum tensor, $T_{\mu\nu}$, linearized gravity has other applications in physics, such as the study of gravitational waves. It is applicable when the metric can be expressed as the Minkowski metric plus a perturbation:

$$g_{\mu\nu} = \eta_{\mu\nu} + h_{\mu\nu}, \tag{5.1}$$

where $h_{\mu\nu}$ is raised and lowered with $\eta_{\mu\nu}$. In order to find the energy-momentum tensor, one must use $h_{\mu\nu}$ rather than $g_{\mu\nu}$ in Einstein's field equations (2.6). Doing so, keeping the equations at first order, yields

$$8\pi T = \partial^\rho \partial_{(\mu} h_{\nu)\rho} - \frac{1}{2}\partial^\rho \partial_\rho h_{\mu\nu} - \frac{1}{2}\partial_\mu \partial_\nu h - \frac{1}{2}\eta_{\mu\nu}\left(\partial^\rho \partial^\sigma h_{\rho\sigma} - \partial^\rho \partial_\rho h\right). \tag{5.2}$$

Because of gauge freedom, we can choose to redefine $h_{\mu\nu}$ in a way that simplifies these equations

$$\bar{h}_{\mu\nu} = h_{\mu\nu} - \frac{1}{2}h\eta_{\mu\nu}, \tag{5.3}$$

$$h = h^a_a = \eta^{a\nu}h_{a\nu}, \tag{5.4}$$

so now we have

$$8\pi T_{\mu\nu} = -\frac{1}{2}\partial^\rho\partial_\rho\bar{h}_{\mu\nu} + \partial^\rho\partial_{(\mu}\bar{h}_{\nu)\rho} - \frac{1}{2}\eta_{\mu\nu}\partial^\rho\partial^\sigma\bar{h}_{\rho\sigma}. \tag{5.5}$$

Furthermore, if we choose the Lorentz gauge,

$$\partial^\nu\bar{h}_{\mu\nu} = 0, \tag{5.6}$$

the equations simplify to

$$\partial_a\partial^a\bar{h}_{\mu\nu} = -16\pi T_{\mu\nu}. \tag{5.7}$$

If not already satisfied, the gauge (5.6) is fulfilled by finding a term ϵ_μ and adding it to $h_{\mu\nu}$ in the following way:

$$h_{\mu\nu} \to h_{\mu\nu} + \partial_\mu\epsilon_\nu + \partial_\nu\epsilon_\mu, \tag{5.8}$$

where ϵ_μ is found through

$$\partial^\nu\partial_\nu\epsilon_\mu = -\partial^\nu\bar{h}_{\mu\nu}. \tag{5.9}$$

We give explicit examples of the computation in section 7.1.1.

5.2 Brown–York Tensor

Another way of finding the energy-momentum tensor consists of using the method developed by Brown and York in [19]. In this paper, a bounded region of spacetime is examined and, along with other quantities, the energy-momentum tensor of the surface boundary is found.

To start, the paper examines the evolution of a space-like surface in a fixed time from t' to t''. The boundary of the surface over this time period defines a surface ∂B.

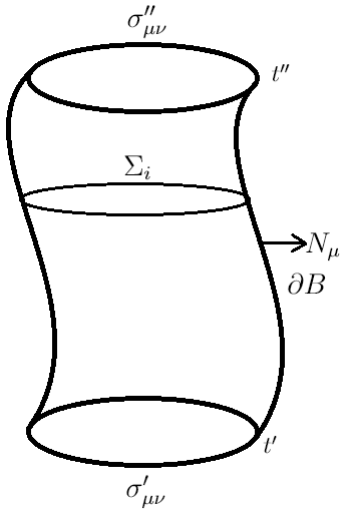

Figure 2: Taking an infinity thin ring at t' and evolving it to the time t''.

This surface ∂B along with the original and finals surfaces at t' and t'' create the full boundary ∂M. This boundary with the inside region, defines a spacetime M[3]. If we take the example of an infinitely thin ring, we can imagine evolving the ring over time to create a tube-like manifold, the surface ∂B, and with the initial and final surface we get a can-like surface, the full boundary ∂M, as shown in fig. 2. The full spacetime M has metric $g_{\mu\nu}$, the boundary ∂B has metric γ_{ab}. The cross section of the surface at each t gives a foliation Σ_i, which has metric $\sigma_{\mu\nu}$, the metric at t' and t'' are denoted as $\sigma'_{\mu\nu}$ and $\sigma''_{\mu\nu}$, respectively. The paper finds the stress-energy tensor through a Hamilton-Jacobi approach and so the action is examined. To have a valid action, one must ensure that when extremizing the action, the boundary terms go to zero. One way of doing this is fixing the metric γ_{ab} on ∂B, as well as $\sigma'_{\mu\nu}$ and $\sigma''_{\mu\nu}$. The action in this case is

$$S = \frac{1}{16\pi}\int_M d^d x\sqrt{-g}R + \frac{1}{8\pi}\int_{t'}^{t''} d^{d-1}x\sqrt{\sigma}\mathcal{K} - \frac{1}{8\pi}\int_{\partial B} d^{d-1}x\sqrt{-\gamma}K + S^m, \qquad (5.10)$$

where S^m is the matter action, $\sigma = \sigma^\mu_\mu$, $\gamma = \gamma^a_a$, R is the intrinsic curvature, $\mathcal{K}$ is the trace of the extrinsic curvature on $\sigma_{\mu\nu}$, and K is the same but on γ_{ab}. In this thesis we only care about the boundary ∂B, so we look at the part of the action concerning γ_{ab}

[3]We use a slightly different notation than the original paper; our ∂B is their ${}^3B$, and our $\sigma_{\mu\nu}$ is their $h_{\mu\nu}$.

which, when extremizing the action gives:

$$\delta S_\gamma = \int_{\partial B} d^{d-1}x \pi^{ab} \delta\gamma_{ab}, \tag{5.11}$$

where π^{ab} is the gravitational momentum conjugate to γ_{ab}. There is an ambiguity in the action which allows for the subtraction of a term S^0, depending only on γ_{ab}, resulting in a new action $S' = S - S^0$. The result of adding such a term is that the energy is shifted. Extremizing this term gives

$$-\delta S^0 = \int_{\partial B} d^{d-1}x \frac{\delta S^0}{\delta\gamma_{ab}} \delta\gamma_{ab} \equiv \int_{\partial B} d^{d-1}x \pi_0^{ab} \delta\gamma_{ab}, \tag{5.12}$$

so in total it becomes

$$\delta S'_\gamma = \int_{\partial B} d^{d-1}x \left(\pi^{ab} - \pi_0^{ab}\right) \delta\gamma_{ab}. \tag{5.13}$$

With this, we can define the energy-momentum tensor on the boundary ∂B as

$$T^{ab} = \frac{2}{\sqrt{-\gamma}} \frac{\delta S}{\delta\gamma_{ab}}, \tag{5.14}$$

and, because we can write the variation in the action as

$$\frac{\delta S}{\delta\gamma_{ab}} = \pi^{ab} - \pi_0^{ab}, \tag{5.15}$$

we write the energy-momentum tensor as

$$T^{ab} = \frac{2}{\sqrt{-\gamma}} \left(\pi^{ab} - \pi_0^{ab}\right). \tag{5.16}$$

Rather than γ_{ab}, we can define these quantities in terms of $h_{\mu\nu}$, given by equation (2.12). If we have the metric $g_{\mu\nu}$, then we can define

$$h_{\mu\nu} = g_{\mu\nu} - N_\mu N_\nu, \tag{5.17}$$

where N_μ is the vector normal to ∂B. The momentum can then be found through the extrinsic curvature

$$\pi^{\mu\nu} = -\frac{1}{16\pi} \sqrt{-h} \left(K h^{\mu\nu} - K^{\mu\nu}\right), \tag{5.18}$$

where the extrinsic curvature is given by:

$$\begin{aligned} K_{\mu\nu} &= -h_\mu^\alpha \nabla_\alpha N_\nu, \\ K &= h^{\mu\nu} K_{\mu\nu}. \end{aligned} \tag{5.19}$$

So putting everything together, the Brown–York energy-momentum tensor is given by

$$T^{\mu\nu} = -\frac{1}{8\pi}\left(Kh^{\mu\nu} - K^{\mu\nu} - \left(K^{(0)}h^{\mu\nu} - K^{(0)\mu\nu}\right)\right), \tag{5.20}$$

where the $K^{(0)}$ terms are associated with the extra action term S^0. This formula works for surfaces with codimension -1. In general, the extrinsic curvature is given by [5]:

$$K^\rho_{\mu\nu} = h^\lambda_\mu h^\sigma_\nu \nabla_\lambda h^\rho_\sigma, \tag{5.21}$$

the extra index, ρ, gives the radial components of the extrinsic curvature. One can get the two-index tensor by contracting over the radial index with N_μ

$$K_{\mu\nu} = N_\rho K^\rho_{\mu\nu} = N_\rho h^\lambda_\mu h^\sigma_\nu \nabla_\lambda h^\rho_\sigma = -h^\rho_\nu h^\lambda_\mu \nabla_\lambda N_\rho, \tag{5.22}$$

which comes from

$$\begin{aligned} &\nabla_\mu N_\rho h^\rho_\sigma = 0, \\ &N_\rho \nabla_\mu h^\rho_\sigma + h^\rho_\sigma \nabla_\mu N_\rho = 0. \end{aligned} \tag{5.23}$$

As a preview of the calculations to be done in future sections, we mention that in our case, $K^{(0)}$ refers to the extrinsic curvature of flat space, which corresponds to taking $r_o \to 0$. We want to find the tensor on the boundary, which corresponds to the worldvolume of the quantity of interest. To do so, we must integrate out the spherical coordinates of the stress tensor to put in on the worldvolume [1]

$$T_{ab} = \int_{S_{n+1}} T^{(BY)}_{ab}. \tag{5.24}$$

6 Fluid Gravity Correspondence

Throughout this thesis we repeatedly find analogues between gravity and fluids, so it is worthwhile to examine the fluid gravity correspondence. In fact, in section 7.3, this correspondence, in conjunction with the AdS/Ricci-flat correspondence, is used to examine the second order correction of a boosted brane metric. Originally explored in [20], the fluid gravity correspondence shows that exploiting the AdS/CFT correspondence in the long wavelength regime, near equilibrium, gives rise to black hole solutions dual to fluid solutions.

We provide a summary of [21], which gives a good overview of this correspondence and the tools required to explore it.

6.1 Fluids

In this context, fluid dynamics is defined as being "the low energy effective description of any interacting quantum field theory," valid for long wavelength fluctuations. To understand this in more depth, one can imagine a system at thermal equilibrium which is then perturbed by allowing fluctuations in the thermodynamic variables. Provided the wavelengths of the fluctuations are large in comparison to the local energy density or temperature, at any point in the system one would find the temperature to be constant in the domain around the point. Each domain will have different values for the thermodynamic variables; the interactions between these domains and their thermodynamic variables is described using fluid dynamics.

To take the hydrodynamic limit of an interacting QFT, one should examine the system at length scales large compared to the characteristic length scale of the system, given by the mean free path length, ℓ_{mfp}. The dynamical charges of the system are given in terms of the energy-momentum tensor $T_{\mu\nu}$, and the charge current J_μ. The dynamical equations are then given by the conservation equations

$$\nabla_\mu T^{\mu\nu} = 0, \qquad \nabla_\mu J^\mu_I = 0, \tag{6.1}$$

where I indexes the conserved charges of the system.

A QFT is defined as living on a d-dimensional spacetime M with metric $g_{\mu\nu}$ described by coordinates x^μ. We seek the energy-momentum tensor and charge currents in terms of the dynamical degrees of freedom of the system, so the system can be described using the dynamical equations. These variables are the local energy density ε, charge densities q_I, fluid velocity u_μ, pressure P, temperature T and chemical potentials μ_I.

6.1.1 Ideal Fluids

An ideal isotropic fluid is a fluid with no viscosity that is incompressible. In this case, the energy-momentum tensor takes the well known form of

$$T^{\mu\nu}_{(0)} = \varepsilon u^\mu u^\nu + P\left(g^{\mu\nu} + u^\mu u^\nu\right). \tag{6.2}$$

When the fluid is at rest, the energy-momentum tensor is diagonal with $T_{00} = \varepsilon, T_{ii} = P$. The charge currents are

$$J^\mu_{(0)} = q_I u^\mu. \tag{6.3}$$

It is interesting to look at the entropy current, which is simply given in terms of the entropy density $s(x)$

$$\left(J^\mu_S\right)_{(0)} = s u^\mu, \tag{6.4}$$

for an ideal fluid, it is conserved

$$\nabla_\mu \left(J^\mu_S\right)_{(0)} = 0. \tag{6.5}$$

Ideal fluids are used in many fields across physics to model and probe ideal scenarios, for example, modeling the evolution of the universe.

6.1.2 Dissipative Fluids

To be more in tune with the real world, we look at dissipative fluids. To describe dissipative hydrodynamics, dissipative terms are added: $\Pi^{\mu\nu}$ to the ideal energy-momentum

tensor and Υ^μ to the ideal charge currents. The next step consists of finding what they are in terms of the variables of the system.

When constructing the Lagrangian in an effective QFT, one must take into account all the possible terms consistent with the symmetries, but there are ways of finding and disregarding unnecessary terms. Here, hydrodynamics is treated as an interacting field theory so this can also be done. In this case the terms that can be disregarded are derivatives of the thermodynamic variables and velocity field. This means the energy-momentum tensor can be found through a gradient expansion. The dissipative components are constrained with the choice of velocity field, to which is imposed

$$\Pi^{\mu\nu}u_\mu = 0, \qquad \Upsilon^\mu u_\mu = 0. \tag{6.6}$$

This ensures that the dissipative contributions are orthogonal to the velocity field. This is known as the Landau frame. To find the dissipative terms of the energy-momentum tensor up to first order, all possible symmetric two-tensors composed of velocity terms must be found, which are obtained by decomposing the gradient

$$\nabla^\nu u^\mu = -a^\mu u^\nu + \sigma^{\mu\nu} + \omega^{\mu\nu} + \frac{1}{d+1}\vartheta P^{\mu\nu}, \tag{6.7}$$

where $\sigma^{\mu\nu}$ is the shear, ϑ is the divergence, $\omega^{\mu\nu}$ is the vorticity, a^μ is the acceleration and P is the orthogonal projector given by

$$\begin{aligned} \vartheta &= \nabla_\mu u^\mu, \\ a^\mu &= u^\nu \nabla_\nu u^\mu, \\ \sigma^{\mu\nu} &= \nabla^{(\mu}u^{\nu)} + u^{(\mu}a^{\nu)} - \frac{1}{d-1}\vartheta P^{\mu\nu}, \\ \omega^{\nu\mu} &= \nabla^{[\mu}u^{\nu]} + u^{[\mu}a^{\nu]}, \\ P^{\mu\nu} &= g^{\mu\nu} + u^\mu u^\nu. \end{aligned} \tag{6.8}$$

We note that, by looking at projections of the conservation equation of the ideal fluid

tensor, one can relate the gradients of the energy density and pressure to those of u^μ

$$\begin{aligned} u^\nu \nabla_\mu (T^{\mu\nu})_{ideal} = 0 \Rightarrow (\varepsilon + P)\nabla_\mu u^\mu + u^\mu \nabla_\mu \varepsilon = 0, \\ P_{\nu\alpha} \nabla_\mu (T^{\mu\nu})_{ideal} = 0 \Rightarrow P^\mu_\alpha \nabla_\mu P + (\varepsilon + P) P_{\nu\alpha} u^\mu \nabla_\mu u^\nu = 0. \end{aligned} \tag{6.9}$$

By applying the Landau frame, one finds the dissipative terms are

$$\Pi^{\mu\nu}_{(1)} = -2\eta\sigma^{\mu\nu} - \zeta\vartheta P^{\mu\nu}, \tag{6.10}$$

where η is the shear viscosity and ζ is the bulk viscosity. The dissipative components of the charge current are found through first order derivative expansions of the energy and charge densities, ε and q_I. The acceleration is eliminated using the zeroth order equation of motion (6.9). In addition to the two terms, in $D = 4$ there is also the possibility of adding a pseudo-vector

$$\ell^\mu = \epsilon^\mu_{\alpha\beta\gamma} u^\alpha \nabla^\beta u^\gamma. \tag{6.11}$$

The first order correction to the charge current is

$$\Upsilon^\mu_{(1)I} = -\tilde{\varkappa}_{IJ} P^{\mu\nu} \nabla_\nu q_J - \tilde{\gamma}_I P^{\mu\nu} \nabla_\nu \varepsilon - \mho_I \ell^\mu, \tag{6.12}$$

where $\tilde{\varkappa}_{IJ}$ is the matrix of charge diffusion coefficients, $\tilde{\gamma}_I$ is the contribution of the energy density to the charge current, and $\mho_I$ are the pseudo-vector transport coefficients. Adding these perturbations to (6.2) and (6.3) give the energy-momentum tensor and charge currents for a generic charged fluid flow up to first order corrections

$$\begin{aligned} T^{\mu\nu} &= \varepsilon u^\mu u^\nu + P\left(g^{\mu\nu} + u^\mu u^\nu\right) - 2\eta\sigma^{\mu\nu} - \zeta\vartheta P^{\mu\nu}, \\ J^\mu &= q_I u^\mu - \tilde{\varkappa}_{IJ} P^{\mu\nu} \nabla_\nu q_J - \tilde{\gamma}_I P^{\mu\nu} \nabla_\nu \varepsilon - \mho_I \ell^\mu. \end{aligned} \tag{6.13}$$

With these higher order terms, the entropy current is no longer conserved. The second law of thermodynamics can be interpreted as entropy having a non-negative divergence, so we must have

$$\nabla_\mu J^\mu_S \geq 0. \tag{6.14}$$

This is to be expected as if the system is perturbed away from equilibrium, the dissipa-

tive equations will allow it to equilibrate again; this process produces entropy. While the equations for dissipative fluids are not as simple compared to the ideal case, these complications are necessary to explore physics closer to what we would expect to see in the real world.

6.1.3 Conformal Fluids

As the fluid/gravity correspondence is a subsector of the AdS/CFT correspondence, studying conformally invariant theories is imperative. Again taking the boundary metric $g_{\mu\nu}$ defined on a d-dimensional spacetime M, a Weyl transformation is made

$$g_{\mu\nu} = e^{2\phi}\tilde{g}_{\mu\nu}. \tag{6.15}$$

A tensor Q is conformally invariant if it transforms under Weyl transformations of the metric as

$$Q = e^{-\omega\phi}\tilde{Q}, \tag{6.16}$$

where ω is the conformal weight of the tensor. To be conformally invariant, $T_{\mu\nu}$ must be traceless and transform with weight $d+2$ as

$$T^{\mu\nu} = e^{-(d+2)\phi}\tilde{T}^{\mu\nu}, \tag{6.17}$$

while the charge currents transform with weight d as

$$J^{\mu} = e^{-d\phi}\tilde{J}^{\mu}. \tag{6.18}$$

The energy-momentum tensor of an ideal conformal fluid is

$$T^{\mu\nu}_{(0)} = \alpha T^{d}\left(g^{\mu\nu} + d\, u^{\mu}u^{\nu}\right), \tag{6.19}$$

where T is the temperature and α is a dimensionless normalization constant depending on the CFT. For higher order corrections, one must find the higher order operators that transform homogeneously. At first order, a viscous conformal fluid has, in terms of the

variables defined in (6.8),

$$\begin{aligned} T^{\mu\nu}_{(1)} &= \alpha T^d \left(g^{\mu\nu} + d\, u^\mu u^\nu\right) - 2\eta\sigma^{\mu\nu}, \\ J_{(1)} &= q_I u^\mu - \varkappa_{IJ} P^{\mu\nu}\nabla_\nu\left(\frac{\mu_J}{T}\right) - \mho\ell^\mu. \end{aligned} \tag{6.20}$$

The next higher order corrections can be found using the same procedure, but in order to do calculations more generally, it is useful to find a Weyl covariant derivative $\mathcal{D}_\mu$.

We start by looking at the conformal class of metrics on the background manifold M. The background with this class of metrics is denoted as $(M, \mathcal{C})$. On this background, $\mathcal{D}_\mu$ is built with Weyl connection ∇^{Weyl}_α that obeys

$$\nabla^{Weyl}_\alpha g_{\mu\nu} = 2A_\alpha g_{\mu\nu}, \tag{6.21}$$

where A_μ is a one-form to be determined. $\mathcal{D}_\mu$ takes the form of

$$\mathcal{D}_\mu = \nabla^{Weyl}_\alpha + \omega A_\mu. \tag{6.22}$$

Using the fact that the Weyl covariant derivative is transverse, traceless and obeys $\mathcal{D}_\alpha g_{\mu\nu} = 0$, A_μ is found to be

$$A_\mu = u^\lambda \nabla_\lambda u_\mu - \frac{1}{d-1} u_\mu \nabla^\lambda u_\lambda. \tag{6.23}$$

One can rewrite the gradient terms in the stress energy tensor using this derivative, such as $\sigma^{\mu\nu} = \mathcal{D}^{(\mu}u^{\nu)}$. The conservation equation for the stress tensor (6.1) maintains its form and simply becomes $\mathcal{D}_\mu T^{\mu\nu} = 0$.

6.2 Correspondence to Gravity

Having reviewed the relevant fluid topics, the next step is to examine the correspondence to gravity.

We take a d-dimensional theory on a background $\mathcal{B}$ dual to string theory on an asymptotically AdS_{d+1} spacetime; type IIB string theory on $\mathrm{AdS}_5 \times S^5$ dual to $N = 4$

SYM is an example of this. In $N = 4$ SYM, there are two dimensionless parameters: the 't Hooft parameter λ, and the rank of the gauge group N. When these two parameters are large, the dynamics of the theory are described by classical gravity. Taking a universal subsector of the theory allows us to focus on the dynamics of the energy-momentum tensor. The dynamics in question are those of Einstein gravity in AdS space, which has action

$$S_{bulk} = \frac{1}{16\pi} \int d^{d+1}x\sqrt{-g}(R - 2\Lambda), \tag{6.24}$$

and for a metric $g_{\mu\nu}$ on the boundary $\mathcal{B}$, the bulk geometry at zeroth order is

$$ds^2 = \frac{1}{z^2}\left(dz^2 + g_{\mu\nu}dx^\mu dx^\nu\right), \tag{6.25}$$

which can be thought of as asymptotically AdS. To look at hydrodynamics, one needs to be in a long-wavelength regime, and the field theory must be in local thermal equilibrium at a high temperature phase. If these constraints are satisfied, the boundary metric is locally flat, as variations of the metric are small compared to the temperature scale. When finding the hydrodynamic dual, curvature terms do not need to be considered until second order in the gradient expansion, because these curvature terms are second order derivatives.

The geometry dual to a thermal field theory in Minkowski space is that of an AdS_{d+1} Schwarzschild black hole, with the temperature given by $T = \frac{dr_+}{4\pi}$. This family of solutions is characterized by the radius r_+, unless it is boosted in which case it has d parameters according to the boosts, with metric

$$ds^2 = \frac{dr^2}{r^2 f\left(br\right)} + r^2\left(-f\left(br\right)u_\mu u_\nu + P_{\mu\nu}\right)dx^\mu dx^\nu, \tag{6.26}$$

where $f(r) = \frac{1}{1-\frac{1}{r^d}}$. These boosts can also be written as

$$\begin{aligned} u^\nu &= \frac{1}{\sqrt{1-\beta^2}}, \\ u^i &= \frac{\beta_i}{\sqrt{1-\beta^2}}, \\ \beta^2 &= \beta_j \beta^j, \end{aligned} \tag{6.27}$$

with the β_i's being constant. The energy-momentum tensor of this metric is that of an ideal conformal fluid, equation (6.19), with $\alpha = \frac{\pi^d}{16\pi G_N^{(d+1)}}$. The solution is stationary and so it is at a global thermal equilibrium, but the system must be perturbed in order to describe hydrodynamics. This perturbation is achieved by allowing b and β_i to depend on the boundary coordinates. Provided that the variations of the metric caused by this dependency remain small, a solution can be found.

The Weyl covariant form of the boosted AdS_{d+1} Schwarzschild black hole is used, using ingoing Eddington–Finkelstein coordinates, where this transformation is shown in detail in Appendix D.1, to ensure that the metric is regular at the horizon

$$ds^2 = -2u_\mu dx^\mu \left(dr + rA_\mu dx^\mu\right) + r^2 \left(1 - f(rb)\right) u_\mu u_\nu dx^\mu dx^\nu + r^2 g_{\mu\nu} dx^\mu dx^\nu. \tag{6.28}$$

Now, b and β are promoted to functions varying on the boundary coordinates, with the resulting metric denoted as $G^{(0)}_{\mu\nu}$. With these fluctuations, $G^{(0)}_{\mu\nu}$ is not necessarily a solution to Einstein's equations but in the case of slowly varying β_i and b, as long as they satisfy the equations of boundary fluid dynamics, we can say that $G^{(0)}_{\mu\nu}$ is a good approximate solution. Using a small parameter ϵ to keep track of the number of derivatives, the solution up to second order will take the form of

$$G \approx G^{(0)}_{\mu\nu}\left(\beta_i, b\right) + \epsilon\, G^{(1)}_{\mu\nu}\left(\beta_i, b\right) + \epsilon^2\, G^{(2)}_{\mu\nu}\left(\beta_i, b\right), \tag{6.29}$$

and, as β_i and b are functions of ϵx^μ, they can be expanded as

$$\begin{aligned} \beta_i &\approx \beta_i^{(0)} + \epsilon\, \beta_i^{(1)}, \\ b &\approx b^{(0)} + \epsilon\, b^{(1)}. \end{aligned} \tag{6.30}$$

To aid with calculations, the background field gauge is chosen

$$G_{rr} = 0, \qquad G_{ru} \propto u_\mu, \qquad Tr\left(G^{(0)^{-1}}_{\mu\nu} G^{(n)}_{\mu\nu}\right) = 0 \quad \forall n > 0. \tag{6.31}$$

Plugging (6.29) into Einstein's equations gives $d(d+1)/2$ dynamical equations and d constraint equations. The metric solving these equations up to second order is of the form

$$ds^2 = -2S(r,x)u_\mu(x)dx^\mu dr + \chi_{\mu\nu}(r,x)dx^\mu dx^\nu, \tag{6.32}$$

where $S(r,x)$ and $\chi_{\mu\nu}(r,x)$ can be written as a perturbative expansion and are given explicitly in equation (F.2). It is raised and lowered with the boundary metric

$$g_{\mu\nu} = \lim_{r\to\infty} \frac{1}{r^2}\chi_{\mu\nu}(r,x). \tag{6.33}$$

To include Weyl covariance, a different form of the metric is used

$$ds^2 = -2u_\mu(x)dx^\mu \left(dr + \mathcal{B}_\nu(r,x)dx^\nu\right) + \mathcal{G}_{\mu\nu}(r,x)dx^\mu dx^\nu, \tag{6.34}$$

where the explicit form of $\mathcal{B}$ and $\mathcal{G}$ are written in equation (F.3). The boundary energy-momentum tensor can now be found using the method of Brown and York, as summarized in section 5.2. The metric used in these calculations is the metric found on the hypersurface at $r = \Lambda_c$.

This technique is quite powerful for finding higher order perturbations when solutions are known on one side of the correspondence. In section 7.3, we review an application of this correspondence together with the Ads/Ricci-flat correspondence.

7 Myers–Perry Black Holes as Blackfolds

This section consists of the main work of this thesis. We apply the blackfold approach to the Myers–Perry black hole, verifying the metric and energy-momentum tensor for the ideal case. We then take the metric to first order and compare the metric with known results. We end the section by reviewing second order corrections found in [3].

We start off by explaining the conditions under which the blackfold approach can be applied to Myers–Perry black holes. The first step is identifying the different scales, s and S as described in section 4. One of the black hole's angular momenta is chosen to act as the larger scale, while the radius acts as the smaller scale. In the case of the doubly-spinning Myers–Perry black hole, equation (3.9), defining $a = a_1$ and $b = a_2$, a is chosen which gives the relation $a \gg r+$. The thickness of the disk r_+ is found by taking the largest real root of of the denominator of g_{rr}. The same relation is obtained for the singly-spinning case, equation (3.7). Taking this limit, the black hole flattens out in the worldvolume directions into a rotating disk of larger radius a, fig. 3. The

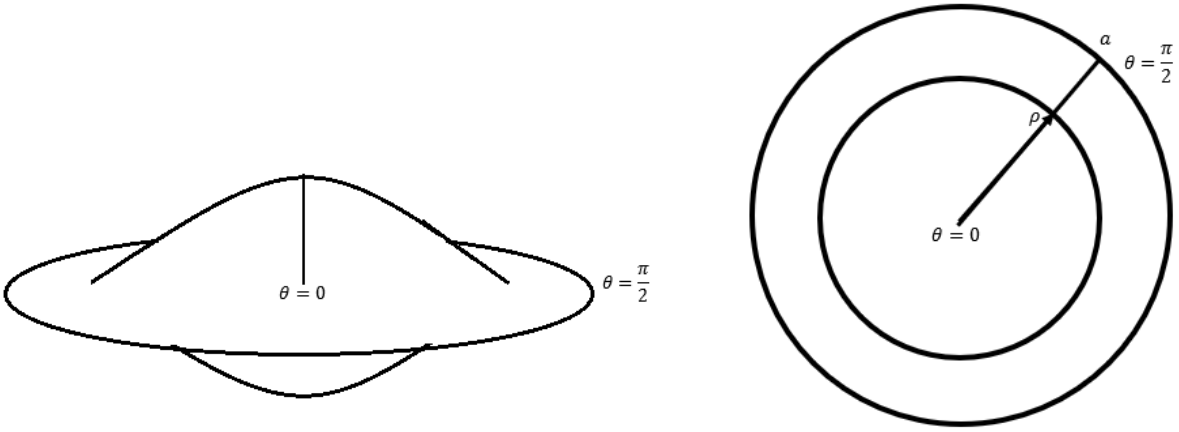

Figure 3: The ultra-spinning Myers–Perry black hole. On the left is the side view and on the right side is the top view.

center of the disk is at $\theta = 0$ and the boundary is at $\theta = \frac{\pi}{2}$. A new variable ρ is defined as $\rho = a \sin\theta$ and can be seen at the radius of the disk at each θ. For the rest of our

calculations, we will focus on the singly-spinning case

$$\begin{aligned} ds^2 = & -dt^2 + \frac{\mu}{r^n \Sigma}(dt - a\sin^2\theta d\phi)^2 + \frac{\Sigma}{\Delta}dr^2 + \Sigma d\theta^2 + (r^2+a^2)\sin^2\theta d\phi^2 \\ & + r^2\cos^2\theta d\Omega_{n+1}^2, \\ \Sigma = & \, r^2 + a^2\cos^2\theta, \qquad \Delta = r^2 + a^2 - \frac{\mu}{r^n}. \end{aligned} \tag{7.1}$$

7.1 Ideal Order

In this section we show the calculations for the ultra-spinning limit in the ideal order case, following the work in [6], and calculate the energy-momentum tensor using linearized gravity and the method of Brown and York.

We begin by applying the ultra-spinning limit, $r_+ \ll a$. The thickness of the disk at each θ is given by $r_o = r_+ \cos\theta$, which turns the limit into $r_o \ll a\cos\theta$. We find r_+ by taking the largest root of Δ

$$0 = r_+^2 + a^2 - \frac{\mu}{r_+^n}, \tag{7.2}$$

which allows μ, the mass parameter, to be written as:

$$\begin{aligned} \mu &= r_+^n \left(r_+^2 + a^2\right), \\ \mu &= \frac{r_o^n}{\cos^n\theta}\left(\frac{r_o^2}{\cos^2\theta} + a^2\right). \end{aligned} \tag{7.3}$$

In order for the blackfold approach to be valid, r_o must vary on scales much larger than its magnitude

$$\begin{aligned} r_o &\ll \frac{1}{\mid r_o'' \mid}, \\ \Longrightarrow r_o &\ll a\cos^2\theta \end{aligned} \tag{7.4}$$

where r_o'' is the curvature. In order to achieve the metric of a black brane everywhere on the horizon, the limit $r \ll a\cos\theta$ must also be taken. We introduce $\epsilon(r,\theta) = \frac{r}{a\cos\theta}$,

which we use as an expansion parameter. With this criteria, Δ, μ and Σ become

$$\begin{aligned} \Delta &\to a^2 - \frac{\mu}{r^n}, \\ \mu &\to \frac{a^2 r_o^n}{\cos^n\theta}, \\ \Sigma &\to a^2 \cos^2\theta, \end{aligned} \tag{7.5}$$

and $\frac{\Sigma}{\Delta}$ simplifies to

$$\frac{\Sigma}{\Delta} \to \frac{a^2\cos^2\theta}{a^2 - \frac{a^2 r_o^n}{r^n\cos^n\theta}} = \frac{\cos^2\theta}{1 - \frac{r_o^n}{r^n\cos^n\theta}}. \tag{7.6}$$

As discussed in section 4, locally a blackfold gives the metric of a boosted brane. In this case, we fix $\theta \to \theta_*$, or alternatively $\rho \to \rho_*$. In order to put the metric in a form resembling the familiar Schwarzschild metric, we make the changes of variables $z = \rho_*\phi$ and $r\cos\theta_* \to r$, which gives

$$ds^2 = -dt^2 + dz^2 + d\rho^2 + \frac{r_0^n}{r^n}\left(\frac{dt}{\cos\theta^*} - tan\theta_* dz\right)^2 + \frac{dr^2}{1 - \frac{r_0^n}{r^n}} + r^2 d\Omega^2_{(n+1)}. \tag{7.7}$$

As expected, this metric corresponds to that of a boosted black brane (4.2) with velocities given by:

$$\begin{aligned} u_t &= sec\theta^*, \\ u_z &= -tan\theta^*. \end{aligned} \tag{7.8}$$

This can also be written in the form of a Lorentz boost:

$$\begin{pmatrix} t' \\ z' \\ \dots \end{pmatrix} = \begin{pmatrix} t \\ z \\ \dots \end{pmatrix} \begin{pmatrix} \gamma & -\gamma v & 0 \\ -\gamma v & \gamma & 0 \\ 0 & 0 & \dots \end{pmatrix} \tag{7.9}$$

with $\gamma = \frac{1}{\sqrt{1-v^2}}$. From this we see $\gamma = \sec\theta^*$ and $v = \sin\theta^*$.

Now, we examine the metric in the region $a \gg r \gg r_o$. This is done by taking the

asymptotic limit $r \gg r_o$, which results in the metric

$$ds^2 = -dt^2 + dz^2 + d\rho^2 + \frac{r_0^n}{r^n}\left(\frac{dt}{\cos\theta^*} - tan\theta_* dz\right)^2 + \left(1 + \frac{r_0^n}{r^n}\right) dr^2 + r^2 d\Omega^2_{(n+1)}. \quad (7.10)$$

As previously mentioned, in the overlap region the Myers–Perry black hole acts as a fluid which can be shown by looking at the stress energy tensor and comparing it to that of a perfect fluid, which is what we will do next.

7.1.1 Linearized Gravity

In this section we use linearized gravity to compute the stress energy tensor as detailed in section 5.1 and compare it to that of a perfect fluid. Rather than using (7.10), it is convenient to switch to isotropic coordinates before taking the asymptotic limit, for computational reasons. This transformation is detailed in Appendix A.

$$n = 1 \textbf{ case}$$

We take the metric (7.7) and make the transformation $r \to r\left(1 + \frac{r_o}{4r}\right)^2$, yielding the metric

$$ds^2 = -dt^2 + d\rho^2 + dz^2 + \frac{r_0}{r\left(1 + \frac{r_o}{4r}\right)^2}\left(\frac{dt}{\cos\theta^*} - tan\theta_* dz\right)^2 + \left(1 + \frac{r_o}{4r}\right)^4 \left(dr^2 + d\Omega^2_{(n+1)}\right). \quad (7.11)$$

Now expanding in the limit of $r \gg r_o$ and switching to Cartesian gives

$$ds^2 = -dt^2 + d\rho^2 + dz^2 + \frac{r_o}{r}\left(\frac{dt}{\cos\theta^*} - tan\theta_* dz\right)^2 + \left(1 + \frac{r_o}{r}\right)\left(dx^2 + dy^2 + dw^2\right), \quad (7.12)$$

where $r = \sqrt{x^2 + y^2 + w^2}$. To find the energy-momentum tensor through linearized gravity, we split up the metric into $g_{\mu\nu} = \eta_{\mu\nu} + h_{\mu\nu}$. The perturbation $h_{\mu\nu}$ is

$$h_{\mu\nu} = \frac{r_0}{r}\left(\frac{dt}{\cos\theta^*} - tan\theta_* dz\right)^2 + \frac{r_o}{r}\left(dx^2 + dy^2 + dw^2\right). \quad (7.13)$$

To apply the Lorentz gauge, which will give an energy-momentum tensor of (5.7), we need to find $\bar{h}_{\mu\nu}$, which requires the trace h given by

$$h = \frac{r_o}{r}\left(-\frac{1}{\cos\theta^{*2}} + \tan\theta_*^2 + 3\right) = 2\frac{r_o}{r}. \tag{7.14}$$

Using equation (5.3), $\bar{h}_{\mu\nu}$ is found to be

$$\bar{h}_{\mu\nu} = \frac{r_o}{r}\left[\left(\frac{1}{\cos^2\theta^*} + 1\right)dt^2 + \left(\tan^2\theta_* - 1\right)dz^2 - 2\frac{\tan\theta_*}{\cos\theta^*}dzdt - d\rho^2\right]. \tag{7.15}$$

Before finding the fluid tensor, the gauge condition (5.6) must be verified. Seeing as $\bar{h}$ only depends on r, and there is no $\bar{h}_{rr}$ component, the gauge condition is satisfied. For example, for $\mu = t$ we have

$$\begin{aligned} &\partial^\nu h_{t\nu} = 0, \\ &\eta^{tr}\partial_r h_{tt} + \eta^{zr}\partial_r h_{zt} = 0. \end{aligned} \tag{7.16}$$

The fluid tensor is now found by taking the Laplacian of $\bar{h}$. Using the property

$$\Delta_{(D-1)} r^{-(D-3)} = -(D-3)\Omega_{(D-2)}\delta^{D-1}(r), \tag{7.17}$$

where D=n+3 [6]. The Laplacian of $\bar{h}_{\mu\nu}$ is

$$\begin{aligned} \partial_a\partial^a\bar{h}_{\mu\nu} &= -\Omega_{(2)}r_o\delta^3(r)\left[\left(\frac{1}{\cos^2\theta^*} + 1\right)dt^2 + \left(\tan^2\theta_* - 1\right)dz^2 \right. \\ &\quad \left. - 2\frac{\tan\theta_*}{\cos\theta^*}dzdt - d\rho^2\right] \qquad (7.18) \\ &= -\Omega_{(2)}r_o\delta^3(r)\left((u_t^2 - \gamma_{tt})dt^2 + 2u_z u_t dzdt + (u_z^2 - \gamma_{zz})dz^2 - d\rho^2\right) \\ &= -\Omega_{(2)}\delta^3(r)r_o(u_\mu u_\nu - \gamma_{\mu\nu}), \qquad (7.19) \end{aligned}$$

giving an energy-momentum tensor of

$$T_{\mu\nu} = \frac{1}{16\pi}\delta^3(r)\Omega_{(2)}r_o(u_\mu u_\nu - \gamma_{\mu\nu}). \tag{7.20}$$

Intuitively, the delta means that we are looking from asymptotically far away, so we

have an infinitesimal black hole.

Now we compare to the perfect fluid tensor, given by equation (4.9). In this case γ^{ab}, the worldvolume metric, is the Minkowski metric. When $n = 1$, the perfect fluid tensor is

$$T_{ab} = \frac{\Omega_{(2)} r_o}{16\pi}(u_a u_b - \gamma_{ab}), \tag{7.21}$$

which matches the result of (7.20).

General n case

Examining the $n = 1$ and $n = 2$ cases, which we compute in appendix B, a pattern emerges. In arbitrary dimensions, starting with

$$ds^2 = -dt^2 + d\rho^2 + dz^2 + \frac{r_o^n}{r^n}\left(u_0 dt + u_1 dz\right)^2 + \left(1 - \frac{r_o^n}{r^n}\right) dr^2 + r^2 d\Omega_{(n+1)}, \tag{7.22}$$

we would expect $h_{\mu\nu}$ to look like

$$h_{\mu\nu} = \frac{r_o^n}{r^n}\left(u_0 dt + u_1 dz\right)^2 + \frac{1}{n}\frac{r_o^n}{r^n}\left(dx_0^2 + ... + dx_{n+1}^2\right), \tag{7.23}$$

which gives

$$\bar{h}_{\mu\nu} = \frac{r_o^n}{r^n}\left(u_0 dt + u_1 dz\right)^2 + \frac{1}{n}dt^2 - \frac{1}{n}dz^2 - \frac{1}{n}d\rho^2, \tag{7.24}$$

and

$$\begin{aligned}
T_{tt} &= n\frac{1}{16\pi}\delta^{n+2}(r)\Omega_{(n+1)} r_o^n \left(u_0^2 + \frac{1}{n}\right), \\
T_{tz} &= n\frac{1}{16\pi}\delta^{n+2}(r)\Omega_{(n+1)} r_o^n u_0 u_1, \\
T_{zz} &= n\frac{1}{16\pi}\delta^{n+2}(r)\Omega_{(n+1)} r_o^n \left(u_1^2 - \frac{1}{n}\right), \\
T_{\rho\rho} &= -n\frac{1}{16\pi}\delta^{n+2}(r)\Omega_{(n+1)} r_o^n \frac{1}{n},
\end{aligned} \tag{7.25}$$

which matches (4.9). Increasing the worldvolume dimensions has no effect on the result. One can see this first by noting that the energy-momentum tensor explicitly depends on n but not on p. The second way to see this is by looking at the computation of h; because

of the property $u_a u^a = -1$, the calculation of h will simply yield $\frac{r_o^n}{r^n}\left(\frac{1}{n}(n+2)-1\right)$, no matter the dimension of p. Knowing this, it is easy to see by following the previous calculations that p does not have an effect anywhere else.

7.1.2 Brown–York

The stress-energy tensor can also be calculated through the method of Brown and York as detailed in section 5.2. This method requires calculating the stress energy tensor on a quasilocal surface. In this case, this surface ∂B is achieved by taking the directions transverse to the worldvolume coordinates very large, as was done to the metric previously when taking the asymptotic limit resulting in (7.10). Using the equation (5.20) to compute the stress energy tensor requires computing the extrinsic curvature $K_{\mu\nu}$ (5.21). To calculate the metric $h_{\mu\nu}$ (not to be confused with $h_{\mu\nu}$ from the linearized gravity section) on the surface, the vector normal to the surface must be found, which only has the radial r component. This is found through:

$$\begin{aligned} N_\mu &= \frac{dr}{\mid N \mid}, \\ g^{\mu\nu} N_\mu N_\nu &= 1, \\ \frac{1}{\mid N \mid^2}\frac{1}{1-\frac{r_o^n}{r^n}} &= 1, \\ N_\mu &= \frac{dr}{\sqrt{1-\frac{r_o^n}{r^n}}}, \end{aligned} \tag{7.26}$$

which yields a metric of

$$\begin{aligned} h_{\mu\nu} &= g_{\mu\nu} - N_\mu N_\nu, \\ h_{\mu\nu} &= -dt^2 + d\rho^2 + dz^2 + \frac{r_0^n}{r^n}\left(\frac{dt}{\cos\theta^*} - tan\theta_* dz\right)^2 + r^2 d\Omega^2_{(n+1)}. \end{aligned} \tag{7.27}$$

We take the $n = 1$ for the remainder of the calculations. The metric (7.27) is equivalent to projecting the spacetime metric onto the surface while keeping r constant, which is

to say using the embedding map

$$X^t = t, \quad X^z = z, \quad X^\rho = \rho, \quad X^r = R, \quad X^\omega = \omega, \quad X^{\omega_2} = \omega_2. \tag{7.28}$$

The form of $h_{\mu\nu}$ yields $h^\mu_\nu = \delta^\mu_\nu$. In addition, using the fact that N_μ has only one component, $N_r = \frac{1}{\sqrt{1-\frac{r_o}{r}}}$, and that r is constant on the surface, the equation for extrinsic curvature (5.21) simplifies to:

$$K_{\mu\nu} = -\frac{1}{\sqrt{1-\frac{r_o}{r}}}\Gamma^r_{\mu\nu}. \tag{7.29}$$

The Christoffels symbols are first calculated using $g_{\mu\nu}$ and then fixed with $r \to R$:

$$\begin{aligned}
\Gamma^r_{tt} &= \frac{\left(1-\frac{r_o}{R}\right) r_o sec^2\theta_*}{2R^2}, \\
\Gamma^r_{zt} &= -\frac{\left(1-\frac{r_o}{R}\right) r_o sec\theta_* tan\theta_*}{2R^2}, \\
\Gamma^r_{zz} &= \frac{\left(1-\frac{r_o}{R}\right) r_o tan^2\theta_*}{2R^2}, \\
\Gamma^r_{rr} &= \frac{r_o}{2R^2\left(1-\frac{r_o}{R}\right)}, \\
\Gamma^r_{\omega\omega} &= -R + r_o, \\
\Gamma^r_{\omega_2\omega_2} &= (-R + r_o)\sin^2\phi.
\end{aligned} \tag{7.30}$$

$K^{(0)}_{\mu\nu}$ is calculated from flat space, which is achieved by setting $r_o = 0$ in $g_{\mu\nu}$ which gives:

$$h^{(0)}_{\mu\nu} = -dt^2 + d\rho^2 + dz^2 + r^2 d\Omega^2_{(2)}. \tag{7.31}$$

Now the normal vector is

$$N^{(0)}_\mu = dr, \tag{7.32}$$

and the equation for $K^{(0)}_{\mu\nu}$ is

$$K_{\mu\nu} = \Gamma^{(0)r}_{\mu\nu}, \tag{7.33}$$

with Christoffel symbols:

$$\begin{aligned}\Gamma^{r}_{\omega\omega} &= -R,\\ \Gamma^{r}_{\omega_2\omega_2} &= -R\sin^2\phi.\end{aligned} \tag{7.34}$$

The Brown–York tensor is

$$T^{ab} = -\frac{1}{8\pi}\left(Kh^{ab} - K^{ab} - \left(K^{(0)}h^{ab} - K^{(0)ab}\right)\right). \tag{7.35}$$

which, plugging in the components found, is

$$\begin{aligned}T^{tt} &= \frac{1}{8\pi}\frac{r_o\left(1+\sec^2\theta_*\right)}{2R^2},\\ T^{zt} &= \frac{1}{8\pi}\frac{r_o\sec\theta_*\tan\theta_*}{2R^2},\\ T^{zz} &= -\frac{1}{8\pi}\frac{r_o\left(1-\tan^2\theta_*\right)}{2R^2},\\ T^{\rho\rho} &= -\frac{1}{8\pi}\frac{r_o}{2R^2},\\ T^{\omega\omega} &= -\frac{1}{8\pi}\left(\frac{r_o}{2R^4}+\frac{r_o\left(-2R+r_o\right)}{2R^4}\right),\\ T^{\omega_2\omega_2} &= -\frac{1}{8\pi}\left(\frac{r_o\csc^2\theta_*}{2R^4}+\frac{r_o\left(-2R+r_o\right)\csc^2\theta_*}{2R^4}\right).\end{aligned} \tag{7.36}$$

The next step is to integrate over S_2:

$$T^{ab} = \int_0^{2\pi}\int_0^{\pi} T^{(BY)ab}R^2\sin\omega d\omega d\omega_2. \tag{7.37}$$

As the asymptotic limit is being taken, $R\to\infty$, after integration the $T^{\omega\omega}$ and $T^{\omega_2\omega_2}$ components vanish. In the end, the energy-momentum tensor is

$$\begin{aligned}T^{tt} &= \frac{r_o\Omega_{(2)}}{16\pi}\left(1+\sec^2\theta_*\right),\\ T^{zt} &= \frac{r_o\Omega_{(2)}}{16\pi}\sec\theta_*\tan\theta_*,\\ T^{zz} &= -\frac{r_o\Omega_{(2)}}{16\pi}\left(1-\tan^2\theta_*\right),\\ T^{\rho\rho} &= -\frac{r_o\Omega_{(2)}}{16\pi},\end{aligned} \tag{7.38}$$

which matches the stress-energy tensor for a perfect fluid (4.9) in $n = 1$ dimensions

$$T^{ab} = \frac{\Omega_{(2)}}{16\pi} r_o \left(u^a u^b - \gamma^{ab}\right). \tag{7.39}$$

With these calculations, we have shown explicitly that, in the ideal case, the energy-momentum tensor of the ultra-spinning Myers–Perry black hole is that of a perfect fluid.

7.2 First Order

7.2.1 Derivation

Starting again with the singly-spinning Myers–Perry black hole (3.7), the metric is taken to first order in $\epsilon(r, \theta)$. Following the same procedure as the ideal order case yields the same results, as the higher order terms are all second order. However, there is a change when taking the coordinate transformations. The procedure is the same until the point where the metric is in the form

$$\begin{aligned} ds^2 = & -dt^2 + a^2 \cos^2\theta d\theta^2 + a^2 \sin^2\theta d\phi^2 + \frac{r_o^n}{r^n \cos^n\theta}\left(\frac{dt}{\cos\theta} - a\frac{\sin^2\theta}{\cos\theta}d\phi\right)^2 \\ & + \cos^2\theta\left(\frac{dr^2}{1 - \frac{r_o^n}{r^n\cos^n\theta}} + r^2 d\Omega_{n+1}\right). \end{aligned} \tag{7.40}$$

First, taking $r' = r\cos\theta$, we have:

$$\begin{aligned} r &= \frac{r'}{\cos\theta}, \\ dr &= \frac{dr'}{\cos\theta} + r d\theta \frac{\sin\theta}{\cos^2\theta}. \end{aligned} \tag{7.41}$$

The next transformation we take is $\rho = a\sin\theta$, which gives:

$$\begin{aligned} \sin\theta &\to \frac{\rho}{a}, \\ \cos\theta &\to, \frac{1}{\sqrt{1-\frac{\rho^2}{a^2}}}, \\ \epsilon(r,\theta) &\to \frac{r}{a\sqrt{1-\frac{\rho^2}{a^2}}} = \epsilon(r,\rho). \end{aligned} \tag{7.42}$$

Now our expansion parameter is in terms of ρ rather than θ. We do calculations in terms of ρ, but will often write the results in terms of $\cos\theta$ and $\sin\theta$ for clarity. When taking the transformation above, dr'^2 becomes

$$dr'^2 = \frac{dr^2}{1-\frac{\rho^2}{a^2}} + 2rdrd\rho\frac{\rho}{a^2\left(1-\frac{\rho^2}{a^2}\right)^2} + d\rho^2\frac{r^2\rho^2}{a^2\left(1-\frac{\rho^2}{a^2}\right)^3}. \tag{7.43}$$

We can see that the $d\rho^2$ term is second order, so we neglect it. We plug this into the metric, but rewrite dr' as dr and write everything in terms of $\sin\theta$ and $\cos\theta$:

$$\begin{aligned} ds^2 = & -dt^2 + a^2\sin^2\theta d\phi^2 + d\rho^2 + \frac{r_o^n}{r^n}\left(\frac{dt}{\cos\theta} - a\frac{\sin^2\theta}{\cos\theta}d\phi\right)^2 \\ & + \frac{dr^2}{1-\frac{r_o^n}{r^n}} + 2\frac{r\sin\theta drd\rho}{\left(1-\frac{r_o^n}{r^n}\right)a\cos^2\theta} + r^2 d\Omega_{n+1}. \end{aligned} \tag{7.44}$$

Compared to the ideal order calculations, the next change is that there is another higher order variable that must be taken into consideration. When doing ideal order calculations, we took θ, and therefore ρ, to be constant. At first order, this gives rise to higher order corrections in $\cos\theta_*$ and $\sin\theta_*$:

$$\begin{aligned} &\rho_* = a\sin\theta_*, \quad \rho = a\sin\theta, \\ &\sin\theta = \sin\theta_* + \frac{\rho-\rho_*}{a}, \\ &\sin^2\theta = \sin^2\theta_* + 2\sin\theta_*\frac{\rho-\rho_*}{a} + \left(\frac{\rho-\rho_*}{a}\right)^2, \\ &\cos^2\theta = \cos^2\theta_* - 2\sin\theta_*\frac{\rho-\rho_*}{a} - \left(\frac{\rho-\rho_*}{a}\right)^2. \end{aligned} \tag{7.45}$$

Now, in addition to $\epsilon(r,\rho)$, the metric will be expanded in terms of $\frac{\rho-\rho_*}{a}$. To simplify, we make the change of coordinates $\rho-\rho_*\to\rho$. Before expanding the metric in ρ, we must take into account the definition of $r_o = r_+\sqrt{1-\frac{\rho^2}{a^2}}$. As it also depends on ρ, we make the transformation back to r_+

$$\begin{aligned} ds^2 = & -dt^2 + a^2\sin^2\theta d\phi^2 + d\rho^2 + \frac{r_+^n\cos^n\theta}{r^n}\left(\frac{dt}{\cos\theta} - a\frac{\sin^2\theta}{\cos\theta}d\phi\right)^2 \\ & + \frac{dr^2}{1-\frac{r_+^n\cos^n\theta}{r^n}} + 2\frac{r\sin\theta dr d\rho}{\left(1-\frac{r_o^n}{r^n}\right)a\cos^2\theta} + r^2 d\Omega_{n+1}. \end{aligned} \tag{7.46}$$

Now, we take ρ to be constant, and making the corrections listed above, the metric becomes

$$\begin{aligned} ds^2 = & -dt^2 + a^2\left(\sin^2\theta_* + 2\sin\theta_*\frac{\rho}{a}\right)d\phi^2 + d\rho^2 \\ & + \frac{r_+^n}{r^n}\left(\frac{dt^2}{\left(\cos^2\theta_* - 2\sin\theta_*\frac{\rho}{a}\right)^{1-\frac{n}{2}}} + \frac{a^2\left(\sin^2\theta_* + 2\sin\theta_*\frac{\rho}{a}\right)^2}{\left(\cos^2\theta_* - 2\sin\theta_*\frac{\rho}{a}\right)^{1-\frac{n}{2}}}d\phi^2\right. \\ & \left. - 2\frac{a\left(\sin^2\theta_* + 2\sin\theta_*\frac{\rho}{a}\right)}{\left(\cos^2\theta_* - 2\sin\theta_*\frac{\rho}{a}\right)^{1-\frac{n}{2}}}dt d\phi\right) \\ & + \frac{dr^2}{1-\frac{r_+^n\left(\cos^2\theta_* - 2\sin\theta_*\frac{\rho}{a}\right)^{\frac{n}{2}}}{r^n}} \end{aligned} \tag{7.47}$$

$$+ 2\frac{r\left(\sin\theta_* + \frac{\rho}{a}\right)dr d\rho}{\left(1-\frac{r_+^n\left(\cos^2\theta_* - 2\sin\theta_*\frac{\rho}{a}\right)^{\frac{n}{2}}}{r^n}\right)a\left(\cos^2\theta_* - 2\sin\theta_*\frac{\rho}{a}\right)} + r^2 d\Omega_{n+1}. \tag{7.48}$$

Now we expand in ρ and get

$$
\begin{aligned}
ds^2 = & -dt^2 + a^2\left(\sin^2\theta_* + 2\sin\theta_*\frac{\rho}{a}\right)d\phi^2 + d\rho^2 \\
& + \frac{r_+^n}{r^n}\Bigg(\left(\frac{\cos^n\theta_*}{\cos^2\theta_*} + (2-n)\frac{\rho}{a}\sin\theta_*\frac{\cos^n\theta_*}{\cos^4\theta_*}\right)dt^2 \\
& + a^2\left(\frac{\cos^n\theta_*}{\cos^2\theta_*}\sin^4\theta_* + \sin^3\theta_*\frac{\rho}{a}\frac{\cos^n\theta_*}{\cos^4\theta_*}\left(4\cos^2\theta + (2-n)\sin^2\theta_*\right)\right)d\phi^2 \\
& - 2a\left(\sin^2\theta\frac{\cos^n\theta_*}{\cos^2\theta_*} + \frac{\rho}{a}\left(2\sin\theta_*\frac{\cos^n\theta_*}{\cos^2\theta_*} + (2-n)\sin^3\theta_*\frac{\cos^n\theta_*}{\cos^4\theta_*}\right)\right)dtd\phi\Bigg) \\
& + \frac{1}{\left(1-\cos^n\theta_*\frac{r_+^n}{r^n}\right)}\left(1 - \frac{\rho}{a}\frac{n\sin\theta_*\cos^n\theta_*\frac{r_+^n}{r^n}}{\cos^2\theta_*\left(1-\cos^n\theta_*\frac{r_+^n}{r^n}\right)}\right)dr^2 \\
& + 2\frac{r}{a}\frac{1}{1-\cos^n\theta_*\frac{r_+^n}{r^n}}\left(\frac{\sin\theta_*}{\cos^2\theta_*} + \frac{\rho}{a}\left(\frac{n\sin^2\theta_*\cos^n\theta_*\frac{r_+^n}{r^n}}{2a\cos^4\theta_*\left(1-\cos^n\theta_*\frac{r_+^n}{r^n}\right)} + \frac{1+\frac{2\sin\theta_*}{\cos^2\theta_*}}{a\cos^2\theta_*}\right)\right)drd\rho \\
& + r^2 d\Omega_{n+1}.
\end{aligned}
\tag{7.49}
$$

The $g_{r\rho}$ term contains second order terms that we drop, and we transform r_+ back to r_o:

$$
\begin{aligned}
ds^2 = & -dt^2 + a^2\left(\sin^2\theta_* + 2\sin\theta_*\frac{\rho}{a}\right)d\phi^2 + d\rho^2 \\
& + \frac{r_o^n}{r^n}\Bigg(\left(\frac{1}{\cos^2\theta_*} + (2-n)\frac{\rho}{a}\frac{\sin\theta_*}{\cos^4\theta_*}\right)dt^2 \\
& + a^2\left(\frac{\sin^4\theta_*}{\cos^2\theta_*} + \frac{\rho}{a}\frac{\sin^3\theta_*}{\cos^4\theta_*}\left(4\cos^2\theta + (2-n)\sin^2\theta_*\right)\right)d\phi^2 \\
& - 2a\left(\frac{\sin^2\theta}{\cos^2\theta_*} + \frac{\rho}{a}\left(2\frac{\sin\theta_*}{\cos^2\theta_*} + (2-n)\frac{\sin^3\theta_*}{\cos^4\theta_*}\right)\right)dtd\phi\Bigg) \\
& + \frac{1}{\left(1-\frac{r_o^n}{r^n}\right)}\left(1 - \frac{\rho}{a}\frac{n\sin\theta_*\frac{r_o^n}{r^n}}{\cos^2\theta_*\left(1-\frac{r_o^n}{r^n}\right)}\right)dr^2 + 2\frac{r}{a}\frac{1}{1-\frac{r_o^n}{r^n}}\frac{\sin\theta_*}{\cos^2\theta_*}drd\rho + r^2 d\Omega_{n+1}.
\end{aligned}
\tag{7.50}
$$

This metric indeed solves Einstein's equations and yields $R_{\mu\nu} = 0$. This metric is also retrieved when taking the metric (7.44) and performing a Taylor expansion around the point ρ_*. Because of this, we can say that the metrics (7.44) and (7.50) are equivalent.

7.2.2 Hydrodynamic Perturbations of Branes

Although finding higher order corrections as done in the previous section is adequate, there are methods to find corrections for general metrics in the near region. One such method is explored in [1]. The idea behind it is that black branes, having thermodynamic behaviour, should be describable by an effective hydrodynamic theory. The paper finds the correction terms through a generic hydrodynamic-type perturbation of the black brane. As stated previously, the energy-momentum tensor of a boosted black brane is asymptotically that of a perfect fluid, depending on the pressure P, and the energy density ε. These quantities can be found through the temperature T of the black hole and the expansion parameter is proportional to T^{-1}. For a vacuum brane, r_o is the inverse of T, so r_o can be used for the expansion, as is done in this thesis.

In this perturbation r_o and u^a are no longer uniform, as opposed to at ideal order, varying with respect to the worldvolume coordinates σ^a and become $r_o(\sigma)$ and $u^a(\sigma)$. Up to first order perturbations, splitting the velocities into the t component and the remaining p worldvolume components, they can be written as

$$\begin{aligned} u^t &= 1 + \mathcal{O}(\epsilon^2), \\ u^b &= \epsilon\sigma^a\partial_a u^b + \mathcal{O}(\epsilon^2), \\ r_o &= r_o + \epsilon\sigma^a\partial_a r_o + \mathcal{O}(\epsilon^2), \end{aligned} \tag{7.51}$$

where ϵ is a derivative counting parameter. With these perturbations, the metric is not guaranteed to be Ricci flat, so a term $f_{\mu\nu}$ is added to compensate. The components of $f_{\mu\nu}$ are found by ensuring that Einstein's equations are satisfied up to first order in ϵ. In order to guarantee horizon regularity, a coordinate transformation to Eddington–Finkelstein coordinates is made. Then, the metric is switched back to Schwarzschild coordinates to ensure asymptotic flatness, which also fixes any remaining constants.
The work done in this paper is generalized in [2] where both the fluid corrections and extrinsic corrections are given. In this paper, the fluid correction terms are shown to

be

$$\begin{aligned} f_{ab}(r) &= \vartheta u_a u_b f_1(r) + \left(\sigma_{ab} + \frac{1}{p}\vartheta P_{ab}\right) f_2(r), \\ f_{ar}(r) &= \vartheta u_a f_3(r) + \dot{u}_a f_4(r), \\ f_{rr}(r) &= \vartheta \frac{1}{1-\frac{r_o^n}{r^n}} f_r(r), \end{aligned} \tag{7.52}$$

where p is the dimension of worldvolume coordinates, ϑ is the divergence of the fluid's velocity, σ_{ab} is the shear of the velocity, and P_{ab} is the orthogonal projector given by

$$\begin{aligned} \vartheta &= D_a u^a, \\ \sigma_{ab} &= P_a^c P_b^d D_{(c} u_{d)} - \frac{1}{p}\vartheta P_{ab}, \\ P_{ab} &= \gamma_{ab} + u_a u_b. \end{aligned} \tag{7.53}$$

The functions f_i are

$$f_1(r) = \frac{r_o}{n(n+1)}\left(2-(n+2)\frac{r_o^n}{r^n}\right)\ln\left(1-\frac{r_o^n}{r^n}\right), \tag{7.54}$$

$$f_2(r) = \frac{2r_o}{n}\ln\left(1-\frac{r_o^n}{r^n}\right), \tag{7.55}$$

$$f_3(r) = \frac{r_0}{n+1}\frac{1}{1-\frac{r_o^n}{r^n}}\left[\left(\frac{n+1}{n}\frac{r_o^n}{r^n}-\frac{1}{n}\right)\ln\left(1-\frac{r_o^n}{r^n}\right)-\frac{r_o^n}{r^n}\left(n\frac{r_*}{r_o}+1\right)\right]+\delta_{(n-1)}, \tag{7.56}$$

$$f_4(r) = \frac{r_*-r}{1-\frac{r_o^n}{r^n}} - \delta_{(n-1)} r_o \ln\frac{r}{r_o}, \tag{7.57}$$

$$f_r(r) = \frac{r_o}{n+1}\frac{1}{1-\frac{r_o^n}{r^n}}\frac{r_o^n}{r^n}\left(2-\ln\left(1-\frac{r_o^n}{r^n}\right)\right), \tag{7.58}$$

where

$$r_* = \int \frac{dr}{1-\frac{r_o^n}{r^n}}. \tag{7.59}$$

In order to compare to the results we achieved in the previous section, we need to provide the worldvolume metric γ_{ab} and the boosts u^a of the ultra-spinning Myers–Perry black

hole:

$$\begin{aligned} \gamma_{ab} &= -dt^2 + \rho^2 d\phi^2 + d\rho^2, \\ u_t &= \frac{1}{\sqrt{1-\frac{\rho^2}{a^2}}}, \qquad u_\phi = -\frac{\rho^2}{a\sqrt{1-\frac{\rho^2}{a^2}}}. \end{aligned} \tag{7.60}$$

Plugging these values in, ϑ and σ_{ab} turn out to be zero. To see this, the Christoffel symbols are calculated with the worldvolume metric. The only non-zero terms are

$$\begin{aligned} \Gamma^{\phi}_{\phi\rho} &= \frac{1}{\rho}, \\ \Gamma^{\rho}_{\phi\phi} &= -\rho, \end{aligned} \tag{7.61}$$

which gives

$$\begin{aligned} \vartheta &= \partial_a u^a + \Gamma^a_{a\lambda} u^\lambda, \\ \vartheta &= \Gamma^t_{t\lambda} u^\lambda + \Gamma^\phi_{\phi\lambda} u^\lambda + \Gamma^\rho_{\rho\lambda} u^\lambda, \\ \vartheta &= 0, \end{aligned} \tag{7.62}$$

so σ_{ab} simplifies to

$$\sigma_{ab} = P^c_a P^d_b D_{(c} u_{d)}, \tag{7.63}$$

which also gives zero. In the end, the only nonzero perturbation term turns out to be

$$f_{ra} = \dot{u}_a \frac{r_* - r}{1 - \frac{r_o^n}{r^n}} - \delta_{(n-1)} \partial_a r_o \log\left(\frac{r}{r_o}\right), \tag{7.64}$$

where $\dot{u}_a$ is given by

$$\dot{u}_a = u^b D_b u_a. \tag{7.65}$$

Having only t and ϕ components of u_a gives

$$\begin{aligned} \dot{u}_a &= u^t D_t u_a + u^\phi D_\phi u_a, \\ \dot{u}_a &= -u^t \Gamma^\lambda_{ta} u_\lambda - u^\phi \Gamma^\lambda_{\phi a} u_\lambda. \end{aligned} \tag{7.66}$$

The only non-zero component turns out to be

$$\dot{u}_\rho = -\frac{\sin\theta}{a\cos^2\theta} = -\frac{\rho}{a^2}\frac{1}{1-\frac{\rho^2}{a^2}}. \tag{7.67}$$

This gives only an $f_{r\rho}$ perturbation term:

$$f_{r\rho} = -\frac{\rho}{a^2}\frac{1}{1-\frac{\rho^2}{a^2}}\left(\frac{r_*-r}{1-\frac{r_o^n}{r^n}} - \delta_{(n-1)}r_o\log\left(\frac{r}{r_o}\right)\right). \tag{7.68}$$

For $n=1$ we have

$$f_{r\rho} = -\frac{\rho}{a^2}\frac{1}{1-\frac{\rho^2}{a^2}}\left(\frac{r_o\log\left(r-r_o\right)}{1-\frac{r_o}{r}} - r_o\log\left(\frac{r}{r_o}\right)\right). \tag{7.69}$$

The need for the extra log term in the $n=1$ case becomes obvious when expanding with $r\to\infty$

$$\begin{aligned} f_{r\rho} &= -r_o\frac{\rho}{a^2}\frac{1}{1-\frac{\rho^2}{a^2}}\left(\log r - \log r + \log r_o + \frac{r_o}{r}\log r\right) \\ &= -r_o\frac{\rho}{a^2}\frac{1}{1-\frac{\rho^2}{a^2}}\left(\log r_o - \frac{r_o}{r}\log r\right). \end{aligned} \tag{7.70}$$

Without the extra term the $\log(r)$ part would blow up as $r\to\infty$. The other term $\frac{\log(r)}{r}$ also goes to zero as $r\to\infty$.

With the correction, the full metric is

$$\begin{aligned} ds^2 = &\left(\gamma_{ab} + \frac{r_o^n}{r^n}u_a u_b\right)d\sigma^a d\sigma^b + \frac{dr^2}{1-\frac{r_o^n}{r^n}} \\ &+2\dot{u}_\rho\left(\frac{r_*-r}{1-\frac{r_o^n}{r^n}} - \delta_{n,1}r_o\log\frac{r}{r_o}\right)drd\rho + r^2 d\Omega^2_{(n+1)}. \end{aligned} \tag{7.71}$$

This is the same as our previous result, equation (7.44), except with extra terms

$$-2\frac{\rho}{a^2}\frac{1}{1-\frac{\rho^2}{a^2}}\left(\frac{r_*}{1-\frac{r_o}{r}} - \delta_{(n-1)}r_o\log\left(\frac{r}{r_o}\right)\right). \tag{7.72}$$

This difference is not a problem if the metrics can be shown to be the same with a gauge transformation. To verify that this is the case, we look at the entropy. As stated in [2], the entropy of the corrected metric should be the same as for the ideal case. The entropy is proportional to the area [22]

$$A = \int_{(S_{n+1})\cap W} d^{D-2}x\sqrt{\det(g_c)}, \tag{7.73}$$

where g_c is the metric at constant t and r, $(S_{n+1})\cap W$ is the surface over the worldvolume and the polar coordinates, and we integrate over the remaining $D-2$ dimensions. The entropy is then calculated using $S = \frac{1}{4}A$. As we are calculating the area of the event horizon, we send $r \to r_o$, but in Schwarzschild coordinates there is a coordinate singularity. One trick to get around this is to set the dr component to 0. At ideal order in $n = 1$ dimensions, first integrating over the angular part $d\Omega_{n+1}$, we have

$$\begin{aligned} S &= -\frac{1}{4}4\pi \int_0^{2\pi} d\phi \int_0^a d\rho\, r_o^2 \rho \frac{1}{\sqrt{1-\frac{\rho^2}{a^2}}} \\ &= -\pi r_+^2 \int_0^{2\pi} d\phi \int_0^a d\rho\, \rho \sqrt{1-\frac{\rho^2}{a^2}} \\ &= \frac{2}{3}\pi^2 r_+^2 a^2. \end{aligned} \tag{7.74}$$

Because the only gauge term is in $g_{r\rho}$, and we are setting $dr = 0$, the area and entropy are trivially the same. More formally, we would have to switch to Eddington–Finkelstein coordinates to work around the singularity issue. The area of an object does not change based on the coordinates, so after this transformation the result should be the same.

By comparing the entropy we confirm that our metric matches that of [1], so we can use this paper to find the energy-momentum tensor up to first order

$$T_{ab} = \varepsilon u_a u_b + P P_{ab} - \zeta\theta P_{ab} - 2\eta\sigma_{ab}. \tag{7.75}$$

In our case, because θ and σ_{ab} are zero, it turns into that of a perfect fluid, as was in the ideal case.

We will make a brief note about the Brown–York calculation for the energy-momentum

tensor. In the ideal order case, one could find $K_{\mu\nu}$ through a simplified formula (C.1). However, in the first order case, because of the $drd\rho$ term, it is not as simple, and we recommend calculating $h_{\mu\nu}$ using (2.12). In this case, the h_{rr} component is not guaranteed to be zero, and instead, one must check that it tends to zero as $r \to \infty$. One can also verify

$$N^\mu h_{\mu\nu} = 0, \tag{7.76}$$

where N^μ is the normal to the worldvolume, to ensure $h_{\mu\nu}$ is valid.

7.3 Second Order: The AdS Ricci-flat Correspondence

Due to insufficient time, we were unable to compute the second order ultra-spinning Myers–Perry black hole metric. Instead, we turn to [3], in which second order brane perturbations are found by first applying the fluid/gravity correspondence, then the AdS/Ricci-flat correspondence. We expect that solutions found through this method should match what we would find by going to second order in the perturbative expansion of the ultra-spinning Myers–Perry black hole in the near-horizon region. In order to compute this second order metric using this method, only the induced metric γ_{ab} and the velocities u_a must be provided (7.60). Using this, one can find the second order Ricci-flat metric of a perturbed black p-brane.

7.3.1 The Correspondence

In [3], the AdS/Ricci-flat correspondence is presented, which is the duality between solutions in Ricci-flat spacetimes and asymptotically AdS spacetimes, which has applications in studying fluid metrics. The paper uses (μ, ν) indices and functions with hats (ie - $\hat{f}$) to indicate AdS quantities, and (a, b) indices and functions with tildes (ie - $\tilde{f}$) to indicate Ricci-Flat quantities.

The correspondence is applicable to solutions $G_{\mu\nu}$ in AdS space in $d+1$ dimensions that satisfy Einstein's equations of the form

$$ds^2_\Lambda = d\hat{s}^2_{p+2}(r, x; d) + e^{2\hat{\phi}(r,x;d)/(d-p-1)} d\bar{y}^2, \tag{7.77}$$

where $R_{\mu\nu} = -\frac{d}{\ell} G_{\mu\nu}$ and $\Lambda = -\frac{d(d-1)}{2\ell^2}$, and ℓ is the AdS radius. The solution depends on a scalar field $\hat{\phi}\,(r, x; d)$, and $(p+2)$-dimensional metric $\hat{g}\,(r, x; d)$ (corresponding to $d\hat{s}^2_{p+2}$ in (7.77)), which can both explicitly depend on the dimensions d. One can take this solution and construct a Ricci-flat solution by taking $\hat{g}$ and $\hat{\phi}$ and setting $d = -n$

$$\tilde{g}\,(r, x; n) = \hat{g}\,(r, x; -n) \qquad \tilde{\phi}\,(r, x; n) = \hat{\phi}\,(r, x; -n)\,. \tag{7.78}$$

This scalar field $\tilde{\phi}\,(r, x; n)$ and (p+2)-dimensional metric $\tilde{g}\,(r, x; n)$, again both able to depend explicitly on n, yield a Ricci-Flat solution ($R_{ab} = 0$), in $D = p + n + 3$ dimensions, of the form

$$ds_0^2 = e^{2\tilde{\phi}(r,x;n)/(d-p-1)} \left(d\tilde{s}^2_{p+2}\,(r, x; n) + \ell^2 d\Omega^2_{n+1} \right). \tag{7.79}$$

The correspondence also goes the other way, starting with Ricci-Flat space and taking $n = -d$ to arrive at a solution with negative cosmological constant. In this case, $\bar{y}$ denotes a $(d-p-1)$-torus but can be generalized to any $(d-p-1)$-dimensional compact Ricci-flat manifold. Likewise, Ω denotes a unit $(n+1)$-sphere, but can be generalized to any $(n+1)$-dimensional compact Einstein manifold with constant positive curvature. An Einstein manifold is a manifold with Ricci tensor proportional to its metric, Ricci-flat manifolds being included in this definition.

One example of its application is to that of a planar AdS black brane

$$ds^2_\Lambda = \frac{1}{r^2} \left(-f(r) d\tau^2 + \delta_{ij} dx^i dx^j + d\vec{y}^2 + \frac{dr^2}{f(r)} \right), \tag{7.80}$$

with $f(r) = 1 - r^d / r_o^d$, and $\bar{y}$ denoting a torus. Applying the correspondence maps

$$\hat{\phi} = -\ln(r)\,(d-p-1) \to \tilde{\phi} = \ln(r)\,(n+p+1), \tag{7.81}$$

$$d\hat{s}_{p+2} = \frac{1}{r^2} \left(-f(r) d\tau^2 + \delta_{ij} dx^i dx^j + \frac{dr^2}{f(r)} \right) \to d\tilde{s}_{p+2} = \frac{1}{r^2} \left(-f(r) d\tau^2 + d\vec{x}^2 + \frac{dr^2}{f(r)} \right),$$

which gives the Schwarzschild p-brane in Ricci-flat space

$$ds_0^2 = -f(r) d\tau^2 + \frac{dr^2}{f(r)} + \delta_{ij} dx^i dx^j + r^2 d\Omega^2_{n+1}, \tag{7.82}$$

with $f(r) = 1 - r_o^n/r^n$.

7.3.2 Derivation of Second Order Brane

The gravity/fluid correspondence, reviewed in section 6, can be used to find solutions to Einstein's equations in AdS space. At zeroth order in derivatives, these solutions describe planar black holes (7.80), which are given by a velocity u_ν and black hole temperature T. In [3] the metric is presented with derivatives up to second order in u_ν and T on the AdS side, then the correspondence is used to find the metric in Ricci-Flat space. The boundary metric is chosen to be flat. The AdS metric is

$$ds^2_\Lambda = -2u_\mu dx^\mu \left(dr + \mathcal{V}_\nu dx^\nu\right) + G_{\mu\nu} dx^\mu dx^\nu. \tag{7.83}$$

The full form of the metric is shown [3] but for the purpose of this thesis, only the relevant terms, meaning terms relevant for the ultra-spinning Myers–Perry black hole, of the Ricci-flat metric will be shown explicitly.

On the Ricci-flat side, a configuration with a $(d-p-1)$-torus symmetry is required, with $u^\mu = (-\tilde{u}^a, \vec{0})$ and a in $(0, ..., p)$, (the negative sign is for in-going Eddington–Finkelstein coordinates). In this case, G_{yy} is

$$G_{yy} = e^{2\hat{\phi}(r,x;d)/(d-p-1)}, \tag{7.84}$$

which are the components of $G_{\mu\nu}$ along the homogeneous directions $\vec{y}$. In general, the shear σ, and divergence ϑ of the fluid are not zero, but for the velocities we are interested in (of the ultra-spinning Myers–Perry black hole), they are. These properties simplify the metric significantly. Making the change $n = -d$ and writing the components in

terms of $\tilde{u}^a$ rather than u^μ, the Ricci-flat metric is given by

$$\begin{aligned}
ds_0^2 &= \frac{1}{G_{yy}}\left(2\tilde{u}_a dx^a\left(-\frac{dr}{r^2}+\mathcal{V}_b dx^b\right)+G_{ab}dx^a dx^b+d\Omega_{n+1}^2\right),\\
G_{yy} &= \frac{1}{r^2},\\
G_{ab} &= \frac{1}{r^2}\tilde{P}_{ab}-\tilde{\omega}_{a\lambda}\tilde{\omega}_b^{\lambda},\\
R &= -2(n+1)\partial_a A^a-(n+2)(n+1)A_b A^b,\\
\mathcal{V}_a &= \frac{1}{r}A_a-\frac{1}{(n+2)}\left[D_\lambda\omega_a^\lambda+\frac{R\tilde{u}_a}{2(n+1)}\right]+\frac{\tilde{u}_a}{2(\frac{r}{r_o})^n}\left[\frac{1}{r^2}\left(1-\left(\frac{r}{r_o}\right)^n\right)-\frac{1}{2}\tilde{\omega}_{\alpha\beta}\tilde{\omega}^{\alpha\beta}\right],\\
\tilde{\omega}_{ab} &= \tilde{P}_a{}^\alpha\tilde{P}_b{}^\beta\partial_{[\alpha}\tilde{u}_{\beta]},\\
D_\lambda\omega_a^\lambda &= \left(\partial^c+(n+3)A^c\right)\tilde{\omega}_{ac},
\end{aligned} \tag{7.85}$$

where $A_a=\tilde{u}^c\partial_c\tilde{u}_a$ acts as a connection for the local conformal symmetry and $\tilde{\omega}_{ab}$ is the vorticity. All together, the Ricci-flat metric is that of a slowly fluctuating black p-brane, also known as a blackfold, which is what was expected to be found. One can find the energy-momentum tensor $T_{\mu\nu}$ in AdS space and map it to the tensor $\tilde{T}_{ab}$ in Ricci-flat space by taking $T_{\mu\nu}\to-\tilde{T}_{ab}$, $d\to-n$ and $u_a\to-\tilde{u}_a$. The tensor takes the form of a perfect fluid tensor but with extra perturbation terms

$$\begin{aligned}
\tilde{T}_{ab} =&\tilde{\varepsilon}\tilde{u}_a\tilde{u}_b+\tilde{P}\tilde{P}_{ab}-2\tilde{\eta}\tilde{\sigma}_{ab}-\tilde{\zeta}\tilde{\theta}\tilde{P}_{ab}\\
&+2\tilde{\eta}\tilde{\tau}_\omega\left[\tilde{P}_a^c\tilde{P}_b^d\tilde{u}^e\partial_e\tilde{\sigma}_{cd}-\frac{\tilde{\theta}\tilde{\sigma}_{ab}}{n+1}+2\tilde{\omega}^c_{(a}\tilde{\sigma}_{b)c}\right]+\tilde{\zeta}\tilde{\tau}_\omega\left[\tilde{u}^c\partial_c\tilde{\theta}+\frac{1}{n+1}\tilde{\theta}^2\right]\tilde{P}_{ab}\\
&-2\tilde{\eta}r_o\left[\tilde{P}_a^c\tilde{P}_b^d\tilde{u}^\epsilon\partial_\epsilon\tilde{\sigma}_{cd}+\left(\frac{2}{p}+\frac{1}{n+1}\right)\tilde{\theta}\tilde{\sigma}_{ab}+\tilde{\sigma}_a^c\tilde{\sigma}_{cb}+\frac{\tilde{\sigma}^2}{n+1}\tilde{P}_{ab}\right]\\
&-\tilde{\zeta}r_0\left[\tilde{u}^c\partial_c\tilde{\theta}+\left(\frac{1}{p}+\frac{1}{n+1}\right)\tilde{\theta}^2\right]\tilde{P}_{ab}.
\end{aligned} \tag{7.86}$$

where $\tilde{\eta}$ and $\tilde{\zeta}$ are the shear and bulk viscosities, $\tilde{\sigma}_{\mu\nu}$ is the shear, $\tilde{\vartheta}=D_a\tilde{u}^a$ is the fluid divergence, $\tilde{P}_{ab}$ is the orthogonal projector, $\tilde{P}$ is the pressure, $\tilde{\varepsilon}$ is the energy density, and the value of $\tilde{\tau}_\omega=\frac{r_o}{n}H_{-2/n-1}$, where this function is shown in (F.10). The equation

of state is given by

$$\tilde{\varepsilon} = -(n+1)\tilde{P}, \qquad \tilde{\zeta} = 2\tilde{\eta}\left(\frac{1}{p} + \frac{1}{n+1}\right). \tag{7.87}$$

As mentioned before, for the velocities in question of the ultra-spinning Myers–Perry metric (7.60), $\tilde{\sigma}_{ab}$ and $\tilde{\vartheta}$ are zero, which turns the energy-momentum tensor into the ideal fluid tensor, yet again.

As this method works for general boosted branes, we reiterate our expectation that the procedure detailed should yield the same solution as the second order the ultra-spinning Myers–Perry black hole.

8 Gregory–Laflamme instability

When talking about higher dimensional black branes, the Gregory–Laflamme instability often comes up. This instability, originally explored in [23], arises when perturbing higher dimensional black p-branes and demonstrates that they are unstable. We begin by going over the general procedure applied to string theory. Next, we review the black ring case and discuss the results of simulations. We finish by comparing the instability to hydrodynamic perturbations.

8.1 Application to String Theory

The question of stability in black p-branes is especially relevant for string theory, so it is instructive to look at low energy 10-dimensional string theory:

$$ds^2 = -V(r)dt^2 + \frac{dr^2}{V(r)} + r^2 d\Omega^2_{\mathbb{d}-2} + dx^i dx_i, \tag{8.1}$$

where $V(r) = 1 - (r_+/r)^{\mathbb{d}-3}$, $4 \leq \mathbb{d} \leq 10$ and i runs from 1 to $(10 - \mathbb{d})$. The metric is then perturbed with $h_{\mu\nu}$

$$g_{\mu\nu} \to g_{\mu\nu} + h_{\mu\nu}. \tag{8.2}$$

We are looking at solutions to the vacuum Einstein equations, meaning $R_{\mu\nu} = 0$, which, when choosing the transverse trace-free (de Donder) gauge $h^a_a = h^a_{b;a} = 0$, gives the following equation for the perturbation:

$$\Delta_L h_{\mu\nu} = \left(\delta^a_\mu \delta^b_\nu \Box + 2R^{ab}_{\mu\nu}\right) h_{ab}, \tag{8.3}$$

where Δ_L is known as the Lichnerowicz operator and $\Box$ is the d'Alembert operator $\partial_\mu \partial^\mu$. The modes are investigated in Schwarzschild coordinates, but one must switch to Kruskal coordinates on the horizon to test them as the event horizon is singular in Schwarzschild coordinates. To solve the equations, an initial data surface is chosen to end on the future event horizon. By examining the symmetries, a solution to the

perturbation equation is found to exist of the form:

$$h_{\mu\nu} = e^{\Omega t} e^{i\mu_i x^i} \begin{bmatrix} H^{tt} & H^{tr} & 0 & 0 & ... \\ H^{tr} & H^{rr} & 0 & 0 & ... \\ 0 & 0 & K & 0 & ... \\ 0 & 0 & 0 & \frac{K}{\sin^2\theta} & ... \\ \vdots & \vdots & \vdots & \vdots & \ddots \end{bmatrix}, \tag{8.4}$$

for certain values of Ω and μ. With this, the Lichnerowicz equation simplifies to:

$$\left(\Delta_L^{\mathbb{d}} + \sum_i \mu_i^2\right) h_{\mu\nu} = 0, \tag{8.5}$$

with the superscript $\mathbb{d}$ signifying $\mathbb{d}$ dimensions. It is important to ascertain which solutions are purely gauge and which are physical. A pure gauge solution obeys $\Delta_L^{\mathbb{d}} h_{\mu\nu} = 0$, so as long as $\sum_i \mu_i^2$ is not zero, the solution will be physical. A gauge can be chosen so that the Lichnerowicz equations reduce to only one component which we can choose to be H^{tr}, giving a second order ordinary differential equation to solve, which we write explicitly in (F.11). The solutions at infinity and at the horizon are

$$\begin{aligned} h_{tr} &\sim e^{-\sqrt{\Omega^2+\mu_i^2} r}, \\ h_{tr} &\sim (r - r_+)^{-1 \pm r_+ \Omega/(\mathbb{d}-3)}, \end{aligned} \tag{8.6}$$

with boundary conditions requiring that the root is positive and that $\Omega > 0$. In [23], a numerical check is made that confirms an instability exists for small values of Ω and μ_i. The general solution near the horizon is

$$h_{tr} \sim A_+(\mu)\,(r - r_+)^{-1 + r_+\Omega/(\mathbb{d}-3)} + A_-(\mu)\,(r - r_+)^{-1 - r_+\Omega/(\mathbb{d}-3)}. \tag{8.7}$$

Finding $A_+(\mu)$ and $A_-(\mu)$ is difficult but in [23] the ratio $R = A_-/A_+$ was found. There is an instability when $R = 0$, so it is possible to find a range of values of Ω and μ_i for which an instability exists.

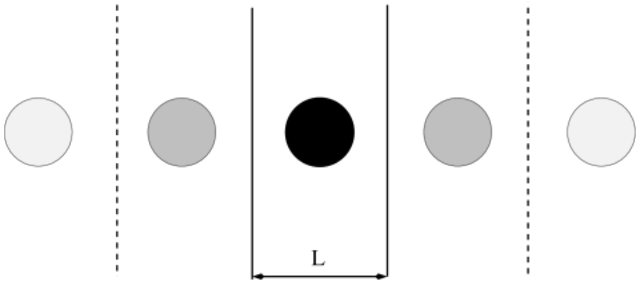

Figure 4: A sketch of the caged black holes case. It is confined along the fifth dimension, beside its mirror images with which it 'interacts' [24].

8.2 Black Rings and Black Holes

In [24], a good overview of the instability is also presented, where thermodynamics is used to motivate the possible existence of an instability. A black hole in 5 dimensions, where one of the dimensions is compactified, has two possible topologies: black holes and black rings. In the case where the radius of the black hole is much smaller than the length of the compactified dimension, L, we have infinite mirror image black holes side by side, along the compactified dimension. These are four-dimensional black holes in five-dimensional space, so the metric is

$$ds^2 = -V(r)dt^2 + \frac{dr^2}{V(r)} + r^2 d\Omega_3^2, \tag{8.8}$$

where it is compactified along one of the $d\Omega_3$ directions and $V(r)$ is a generalization of the $D = 4$ Schwarzschild potential. In the case where L is infinite, $V(r) = \left(1 - \frac{r_+^2}{r^2}\right)$. As the radius of the black hole increases, the black hole turns into a string along the compactified dimensions, which turns the metric into

$$ds^2 = -V(r)dt^2 + V(r)^{-1}dr^2 + r^2 d\Omega_2^2 + dz^2, \tag{8.9}$$

where $V(r) = \left(1 - \frac{r_+}{r}\right)$ and z is the coordinate along which the black hole is extended. These two solutions are typically called "caged black holes" and "nonuniform black strings". The existence of these two solutions raises the question of which is more probable. Giving the solutions the same mass and angular momentum also gives them the same energy, so the energy cannot be used to determine which solution one would

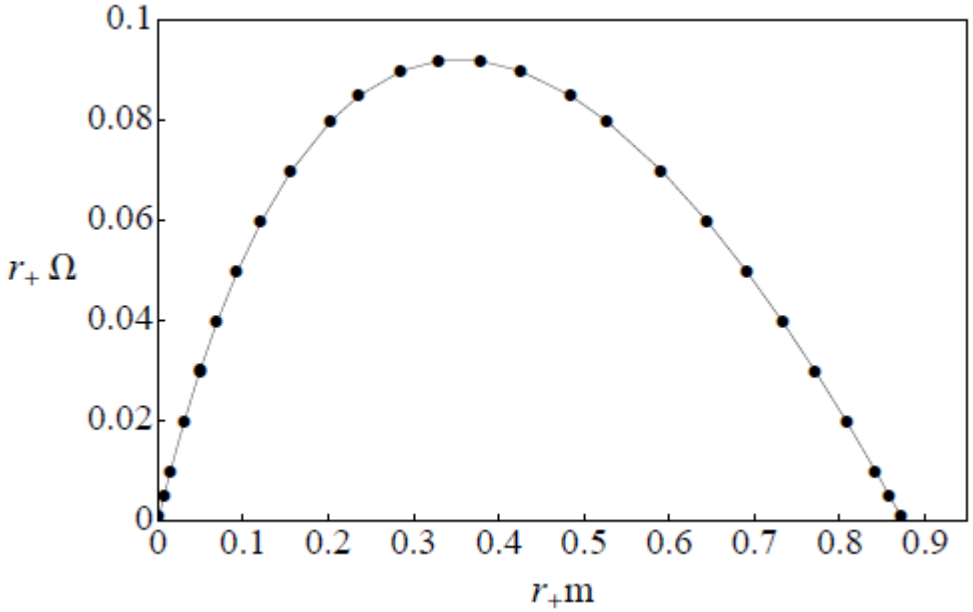

Figure 5: The mode pairs (Ω, m) for which the Gregory–Laflamme instability exists in the case of a black string in 5 dimensions. [24]

expect to find. Instead, one can turn to entropy, as the configuration with the highest entropy is the most probable. The entropy of the black hole, S_{BH}, and of the black string, S_{BS}, are

$$S_{BH} = 4\pi^2 M^2 \sqrt{\frac{8L}{27\pi M}}, \qquad S_{BS} = 4\pi M^2, \tag{8.10}$$

where M is the mass of the black hole and black string set to be equal. Looking at these entropies, one can see that when L becomes large enough, the black hole will be preferred over the black string, which suggests a long wavelength instability in the string. Following the procedures previously detailed, an equation of the form (8.4) is derived that can be solved to find a relation between Ω and $m = \mu_0$. For thermodynamical reasons, an instability can only exist for $r_+ m < 32/37$. One value of Ω is found for each value of m, shown in figure 5. This instability suggests that the black string could segment into black holes, possibly revealing naked singularities.

In [25], a perturbed black ring is numerically evolved. Taking a ring with topology $S_1 \times S_2$, the thickness parameter ν is identified as the ratio between these rings. For very fat rings and rings with $0.2 \lesssim \nu \lesssim 0.6$, perturbing the rings results in a nonaxisymmetric

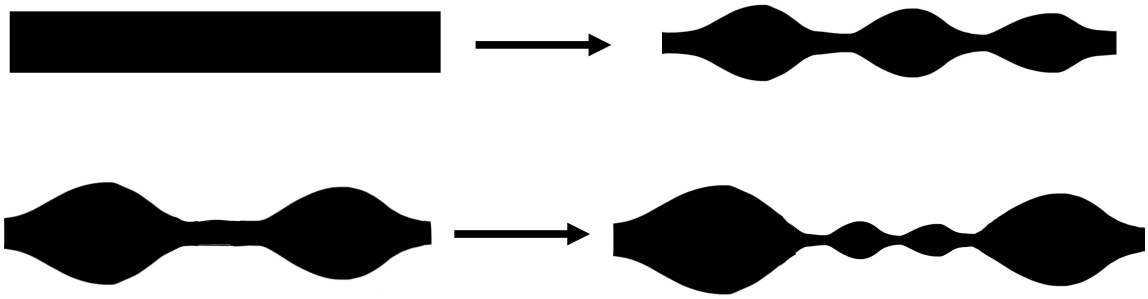

Figure 6: The Gregory–Laflamme instability of a ring.
Top: the thin ring forms the initial bulges connected by thin segments.
Bottom: the thin connecting segments undergo the instability.

instability, commonly referred to as an elastic mode. This instability ends in a Myers–Perry black hole, with a smaller angular momentum than the original ring. In the case of a thin black ring, $\nu \lesssim 0.15$, the Gregory–Laflamme instability would dominate the evolution. In this case, the ring's thickness starts to vary and bulges, connected by thin segments, start to form in the ring. These thin segments could also then be subjected to the instability, creating more bulges connected by even thinner necks, as visualized in fig. 6. While, for insufficient computational resources, the simulations were unable to reach this point, the recursive nature of the simulation suggests that at finite asymptotic time, the thickness of the necks will reach zero, revealing a naked singularity. This scenario was simulated in [26], where one can see the effect visually.

8.3 Fluid Perturbations

In [1], fluid perturbations are compared to the Gregory–Laflamme instability. Considering small static fluid perturbations, a fluid with energy density ε and pressure P is taken from rest, $u^\mu = (1, 0, ...)$, and is perturbed

$$\begin{aligned} &\varepsilon \to \varepsilon + \delta\varepsilon, \qquad P \to P + c_s^2 \delta\varepsilon, \qquad u^\mu = (1, 0, ...) \to (1, \delta u^i), \\ &\delta\varepsilon(t, \sigma^i) = \delta\varepsilon\, e^{i\omega t + i k_j \sigma^j}, \qquad \delta u^i(t, \sigma^i) = \delta u^i e^{i\omega t + i k_j \sigma^j}, \end{aligned} \tag{8.11}$$

where c_s is the speed of sound, i ranges over the space indices and μ ranges over the whole spacetime indices. Plugging these into the viscous fluid equations and linearizing in $\delta\rho$ and δu^i gives the equations one must solve to achieve the solution for a black brane with long-wavelength fluctuations of u^a and r_o. In order to find the dispersion relation $\omega(k)$, one must solve

$$\omega - c_s^2 \frac{k^2}{\omega^2} - i\frac{k^2}{Ts}\left(2\left(1-\frac{1}{p}\right)\eta + \zeta\right) + \mathcal{O}(k^3) = 0, \tag{8.12}$$

where $k = \sqrt{k_i k_i}$ is the wavenumber, s is the entropy, η is the shear viscosity and ζ is the bulk viscosity given by

$$\eta = \frac{s}{4\pi}, \qquad \zeta = 2\eta\left(\frac{1}{p} - c_s^2\right). \tag{8.13}$$

For the energy-momentum tensor of a fluid, the relation between the pressure and energy density gives the speed of sound

$$c_s^2 = \frac{dP}{d\varepsilon} = -\frac{1}{n+1}. \tag{8.14}$$

One can see that c_s is imaginary, which means ω is also imaginary and the sound waves are unstable. Taking $\omega = -i\Omega$,

$$\Omega = \sqrt{-c_s^2}k - \left(\left(1-\frac{1}{p}\right)\frac{\eta}{s} + \frac{\zeta}{2s}\right)\frac{k^2}{T} + \mathcal{O}(k^3). \tag{8.15}$$

Plugging these values in gives

$$\Omega = \frac{k}{\sqrt{n+1}}\left(1 - \frac{n+2}{\sqrt{n+1}}\frac{k}{4\pi T}\right) + \mathcal{O}\left(\frac{k^2}{T^2}\right). \tag{8.16}$$

This equation is expanded in terms of T^{-1} rather than r_o, since $T^{-1} \approx \frac{r_o}{n}$, which suggests we can consider the brane as very hot rather than very thin. In figure 7, we plot (8.16) for $n = 1$ to $n = 7$. One can remark that as n increases, the maximum values of k and Ω decrease; there are fewer possible unstable modes as n increases so hydrodynamics represents more accurately Gregory–Laflamme modes as n grows. This stems from the assumption that the $\frac{k}{T}$ correction terms in (8.16) depend on n in such a

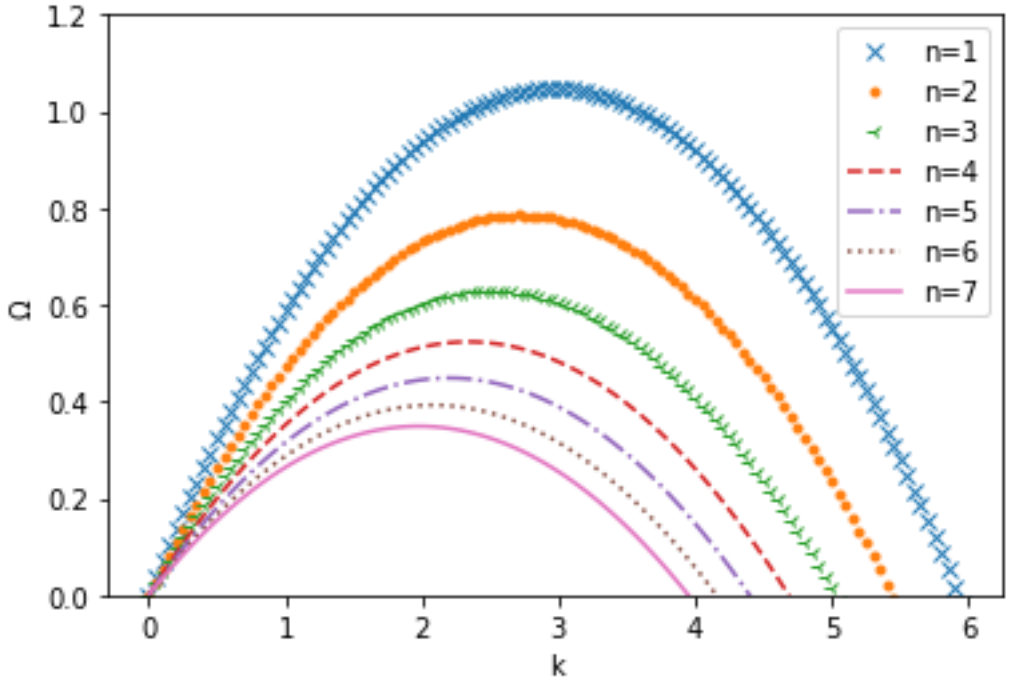

Figure 7: Ω for dimensions $n = 1$ to 7 and fixed T.

way that they tend to 0 as $n \to \infty$. The maximum values scale as $\frac{\Omega}{T} \sim \frac{1}{n}$ and $\frac{k}{T} \sim \frac{1}{\sqrt{n}}$ which we plot in figure 8 and figure 9. To show the agreement with the GL modes, one can find the k value for the 0^{th} mode. With the rescaling

$$\tilde{\Omega} = n\Omega, \qquad \tilde{k} = \sqrt{n}k, \tag{8.17}$$

the equation for Ω becomes

$$\tilde{\Omega} = \tilde{k}\left(1 - \frac{\tilde{k}}{4\pi T}\right), \tag{8.18}$$

which is valid for $0 \leq \tilde{k} \leq 4\pi T$. As $n \to \infty$, the analytical value of k for the GL zero mode k_{GL} becomes

$$k_{GL} \to \frac{4\pi T}{\sqrt{n}}, \tag{8.19}$$

which when plugged into (8.18) yields 0, which further promotes the similarity of the GL instability and fluid perturbations.

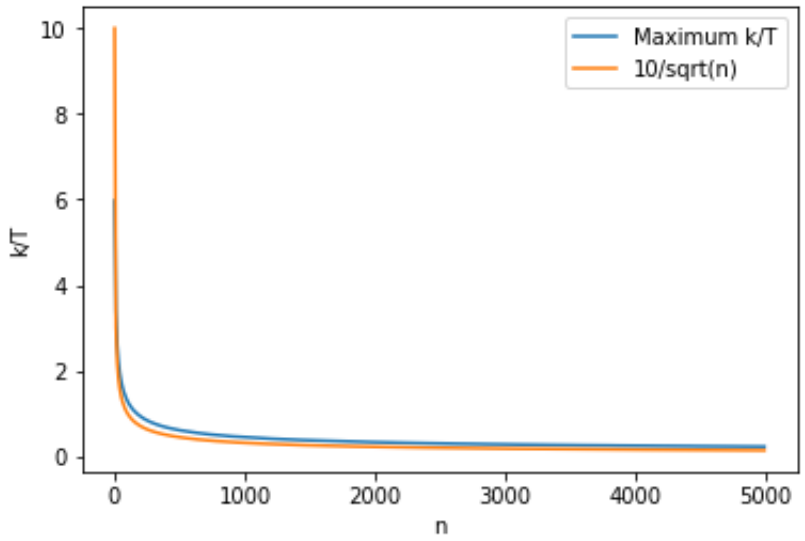

Figure 8: $\frac{k}{T}$ compared to $\frac{10}{\sqrt{n}}$.

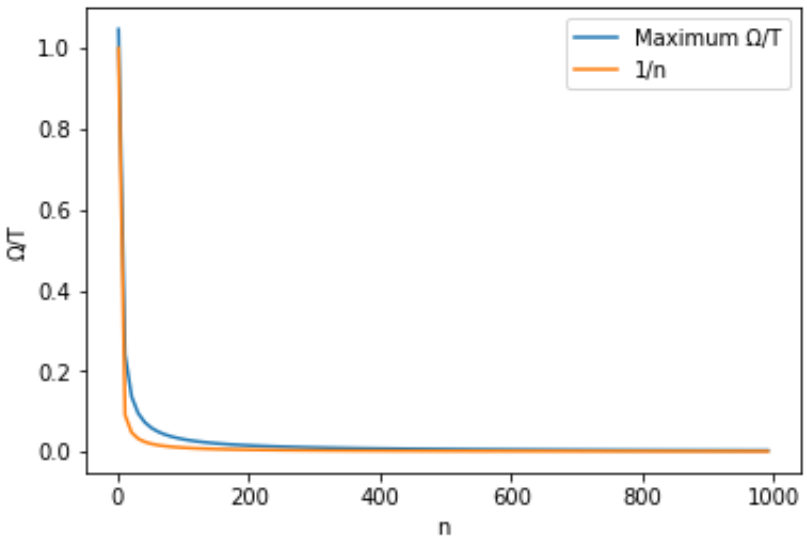

Figure 9: $\frac{\Omega}{T}$ compared to $\frac{1}{n}$.

In [3], which we reviewed in section 7.3, this relation is also explored by examining second order hydrodynamic perturbations of black branes. The energy-momentum tensor in this case is (7.86). The instability resulting from the imaginary speed of sound (8.14) causes the pressure to fluctuate, which causes perturbations in the thickness of the brane. The linearized fluctuations are

$$r_o = \langle r_o \rangle + \delta r_o e^{\Omega t + ikx}, \qquad u_a = \langle u_a \rangle \delta u_a e^{\Omega t + ikx}. \tag{8.20}$$

The energy-momentum tensor is linearized, which consists of dropping products of derivatives. From the conservation of the resulting tensor, the dispersion relation of the speed of sound modes are

$$\Omega = \frac{1}{\sqrt{n+1}} k - \frac{2+n}{n(1+n)} r_o k^2 + \frac{(2+n)\left[2+n\left(2\tilde{\tau}_\omega/r_o - 1\right)\right]}{2n^2(1+n)^{3/2}} r_o^2 k^3 + \mathcal{O}(k^4). \tag{8.21}$$

This dispersion relation resembles the Gregory–Laflamme instability for large n. Taking n large with $\tilde{\Omega} = n\Omega$ and $\tilde{k} = \sqrt{n}k$ yields

$$\tilde{\Omega} = \tilde{k}\left(1 - \frac{\tilde{k}}{4\pi T}\right) - \frac{\tilde{k}}{n}\left(\frac{1}{2} + \frac{\tilde{k}}{4\pi T} - \frac{\tilde{k}^2}{(4\pi T)^2}\right) + \mathcal{O}\left(\frac{1}{n^2}\right). \tag{8.22}$$

One can compare this relation to the one found in [1], equation (8.16). The assumption of [1], that higher order terms will tend to 0 as $n \to \infty$, remains to be true for the second order term in (8.21). From these results, one can again see the relation between gravity and hydrodynamics.

9 Conclusion

When first introduced, the idea of a black hole was quite bizarre but with time and research, black holes have become both a real observable quantity, as well as an invaluable theoretical tool. Physicists have been tasked with examining these extreme objects to garner what they can about their nature and the laws of physics themselves.

For neutral black holes in four dimensions, we have one solution which yields the Schwarzschild black hole in the static case, and the Kerr black hole in the rotating case. Examining black holes in higher dimensions gives us much more freedom in finding black hole solutions. The simplest solution is the higher dimensional Schwarzschild black hole, equation (3.6). Less trivial is the higher dimensional analogue of the Kerr metric, but despite the increased complexity, the solution was found by Myers and Perry. These black hole solutions, shown in equation (3.14) in the odd case, and equation (3.15) in the even case, allow one to construct solutions in $D > 4$ dimensions, spinning in up to $\frac{D-1}{2}$ planes. In higher dimensions, we are not restricted only to these two solutions as more dimensions gives more possible topologies, such as black rings, which we reviewed in section 3.3. However, finding new solutions is challenging.

This is where it is worthwhile to examine the blackfold approach. This technique serves as a useful tool to mold black branes into possible solutions, black rings for example. The example we were most interested in was the case of the Myers–Perry black hole. In the $D \geq 6$ ultra-spinning case, the blackfold approach can be applied. We took the singly-spinning MP black hole and verified in the ideal case that the blackfold approach is applicable. In the near region we confirmed that locally, the solution is that of a boosted black brane, equation (7.7). We then found the metric in the overlap region and found the energy-momentum tensor using both linearized gravity, equation (7.18), and the method of Brown and York, equation (7.38), which both gave us the tensor of a perfect boosted fluid. Examining the ideal case is always enlightening, but examples in the real world are seldom perfect so it is useful to investigate until what point our assumptions hold. For this reason, we recalculated the ultra-spinning MP metric, this time allowing for first order terms. For this calculation, one could imagine that we are in the case where the brane spins a little slower, and where we look at an

area around a point rather than precisely at that point. We found our results matched those of [2], which allowed us to confirm that the energy-momentum tensor remained that of a perfect fluid in the overlap region at first order.

It is not surprising that we find a perfect fluid, as analogies between fluids and gravity are common in physics. One example of this is the fluid/gravity correspondence, which allows one to construct hydrodynamic solutions in d dimensions and map them to gravitational ones in $(d+1)$-AdS space, and vice versa. In [3], the correspondence is used along with the Ads/Ricci-flat correspondence to find second order corrections to black branes. We reviewed these results in section 7.3 and showed the general form of the solution one would expect to achieve when applied to the parameters of the ultra-spinning Myers–Perry black hole.

Another way of looking at this correspondence is through the Gregory–Laflamme instability, reviewed in section 8, which is an instability that affects black branes, causing the radius r_o to vary, becoming thinner in some places and thicker in others. One interesting feature of this instability is its possible endpoint of pinched black holes resulting in naked singularities. The higher order black branes solutions constructed with the duality suffer from sound-mode instabilities. The comparison of the dispersion relation associated to these perturbations to the GL instability has been discussed in both [3], and [1]. In both papers, the match was found to be quite accurate for large n. In section 8.3, we reviewed the discussions of these papers and plotted the dispersion relation found in [1].

As for future work, there is still much to be explored regarding higher dimensional brane calculations. We did not have time to calculate the second order Myers–Perry ultra-spinning black hole but we discussed the form of the second order solution we would expect to find, equation (7.85). One could carry out the calculations explicitly and compare the results with (7.85). Many of our computations were done in Mathematica, using the differential geometry package of [27]. We aimed to extend this package to include the calculation of the Brown–York tensor and were able to write the calculations specifically for black branes of the form (4.2). A package to find this tensor for a general metric, including higher order perturbations, would be useful.

Theoretical black holes continue to allow physicists to probe areas of spacetime inaccessible through observation, partly because it is not guaranteed that these areas exist. Nevertheless, our results allow us to test the limits of our theories and create analogies to others. No matter the topic, if there is an idea to be explored, then a physicist will surely explore it.

A Isotropic Coordinates

Here we will describe the general transformation to isotropic coordinates.

A.1 General Procedure

Following the procedure of [28] Starting with the metric:

$$\left(\eta_{ab} + \frac{r_o^n}{r^n}\right) d\sigma^a d\sigma^b \frac{1}{1-\frac{r_o^n}{r^n}} dr^2 + r^2 d\Omega^2_{(n+1)}, \tag{A.1}$$

the goal is to find an r' such that taking $r \to r'$ will put the polar coordinates in the form of

$$f(r')(dr'^2 + r'^2 d\theta^2 + r'^2 d\Omega^2_{(n+1)}). \tag{A.2}$$

By comparing the two metrics, one can find a relation between r, r' and f:

$$\begin{aligned} r^2 &= r'^2 f(r'), \\ \frac{1}{1-\frac{r_o^n}{r^n}} dr^2 &= f(r') dr'^2, \end{aligned} \tag{A.3}$$

which can then be used to find the relation between r and r':

$$\frac{dr'}{r'} = \frac{dr}{r} \frac{1}{\sqrt{1-\frac{r_o^n}{r^n}}}. \tag{A.4}$$

Integrating this, and using the fact that $r' \to \infty$ as $r \to \infty$, one can find r' and subsequently f.

A.2 n=3 Case

In the n=3 case, the integral evaluates to:

$$\begin{aligned} \frac{2}{3} log\left(\sqrt{r^3 - r_o^3} + r^{\frac{3}{2}}\right) + c = log(r'), \\ \left(\sqrt{r^3 - r_o^3} + r^{\frac{3}{2}}\right)^{\frac{2}{3}} e^c = r', \end{aligned} \tag{A.5}$$

then taking the limit $r \to \infty$

$$\left(2r^{\frac{3}{2}}\right)^{\frac{2}{3}} e^c = r'. \tag{A.6}$$

For r to equal r', e^c must be $2^{\frac{3}{2}}$. Writing r in terms of r' gives:

$$\begin{aligned} r &= r'\left(\frac{r_o^3 2^{\frac{9}{2}}}{r'} + 1\right)^{\frac{2}{3}}, \\ f(r') &= \left(\frac{r_o^3 2^{\frac{9}{2}}}{r'} + 1\right)^{\frac{4}{3}}. \end{aligned} \tag{A.7}$$

Plugging the new r' into the metric transforms it to isotropic coordinates.

B Linearized Gravity for MP black brane in n=2

Here we compute the energy-momentum tensor of the ultra-spinning ideal order Myers–Perry black brane in n=2 dimensions. Once again starting from equation (7.7), the switch to isotropic coordinates in the n=2 case is $r \to r\left(1+\frac{r_o^2}{4r^2}\right)^2$. Employing this transformation and again switching to Cartesian gives

$$\begin{aligned} ds^2 =& -dt^2 + d\rho^2 + dz^2 + \frac{r_o^2}{r^2\left(\frac{r_o^2}{4r^2+1}\right)^2}\left(\frac{dt}{\cos\theta^*} - tan\theta_* dz\right)^2 \\ &+ \left(1+\frac{r_o^2}{4r^2}\right)^2\left(dx_1^2+dx_2^2+dx_3^2+dx_4^2\right). \end{aligned} \tag{B.1}$$

Taking the $r \gg r_o$ limit yields

$$ds^2 = -dt^2+d\rho^2+dz^2+\frac{r_o^2}{r^2}\left(\frac{dt}{\cos\theta^*} - tan\theta_* dz\right)^2+\left(\frac{r_o^2}{2r^2}+1\right)\left(dx_1^2+dx_2^2+dx_3^2+dx_4^2\right), \tag{B.2}$$

for which we find $h_{\mu\nu}$, h and $\bar{h}_{\mu\nu}$:

$$\begin{aligned} h_{\mu\nu} &= \frac{r_o^2}{r^2}\left(\frac{dt}{\cos\theta^*} - tan\theta_* dz\right)^2 + \frac{r_o^2}{2r^2}\left(dx_1^2+dx_2^2+dx_3^2+dx_4^2\right), \\ h &= \frac{r_o^2}{r^2}, \\ \bar{h}_{\mu\nu} &= \frac{r_o^2}{2r^2}dt^2 - \frac{r_o^2}{2r^2}dz^2 + \frac{r_o^2}{r^2}\left(\frac{dt}{\cos\theta^*} - tan\theta_* dz\right)^2 - \frac{r_o^2}{2r^2}d\rho^2 \\ &= \frac{r_o^2}{r^2}\left(u_0^2+\frac{1}{2}\right)dt^2 + u_0u_1\frac{r_o^2}{r^2}dzdt + \frac{r_o^2}{r^2}\left(u_1^2-\frac{1}{2}\right)dz^2 - \frac{r_o^2}{2r^2}d\rho^2 d\rho^2. \end{aligned} \tag{B.3}$$

Taking the Laplacian (7.18) and plugging into equation (5.7)

$$
\begin{aligned}
T_{tt} &= \frac{1}{8\pi}\delta^4(r)\Omega_{(3)}r_o^2\left(u_0^2+\frac{1}{2}\right), \\
T_{tz} &= \frac{1}{8\pi}\delta^4(r)\Omega_{(3)}r_o^2 u_0 u_1, \\
T_{zz} &= \frac{1}{8\pi}\delta^4(r)\Omega_{(3)}r_o^2\left(u_1^2-\frac{1}{2}\right), \\
T_{\rho\rho} &= -\frac{1}{8\pi}\delta^4(r)\Omega_{(3)}r_o^n\frac{1}{2},
\end{aligned}
\tag{B.4}
$$

which matches the perfect fluid equation in 2 dimensions

$$
T^{ab} = \frac{1}{8\pi}\Omega_{(3)}r_o^2(u^a u^b - \frac{1}{2}\gamma^{ab}). \tag{B.5}
$$

C Brown–York Tensor for Schwarzschild Metric

Here we will show explicit computations of the Brown–York tensor calculation for the $D = 4$ Schwarzschild black hole. For the ideal order branes we work with, the equation for the extrinsic curvature is simplified to

$$K_{\mu\nu} = -\frac{1}{\sqrt{f(r)}}\Gamma^{r}_{\mu\nu}. \tag{C.1}$$

For the Schwarzschild metric,

$$ds^2 = -\left(1 - \frac{r_o}{r}\right)dt^2 + \frac{dr^2}{1 - \frac{r_o}{r}} + r^2 d\theta^2 + r^2 \sin^2\theta d\phi^2, \tag{C.2}$$

$f(r) = 1 - \frac{r_o}{r}$. We find $h_{\mu\nu}$ by embedding on a constant R surface:

$$h_{\mu\nu} = -\left(1 - \frac{r_o}{r}\right)dt^2 + r^2 d\theta^2 + r^2 \sin^2\theta d\phi^2. \tag{C.3}$$

The Christoffel symbols for the Schwarzschild metric, taking r constant, are:

$$\Gamma^{r}_{\mu\nu} = \begin{bmatrix} \frac{(1-\frac{r_o}{R})r_o}{2R^2} & 0 & 0 & 0 \\ 0 & \frac{r_o}{2R^2(1-\frac{r_o}{R})} & 0 & 0 \\ 0 & 0 & -R(1-\frac{r_o}{R}) & 0 \\ 0 & 0 & 0 & -R(1-\frac{r_o}{R})\sin^2\theta \end{bmatrix}, \tag{C.4}$$

which yields

$$K_{\mu\nu} = \begin{bmatrix} \frac{-\sqrt{1-\frac{r_o}{R}}r_o}{2R^2} & 0 & 0 & 0 \\ 0 & 0 & 0 & 0 \\ 0 & 0 & R\sqrt{1-\frac{r_o}{R}} & 0 \\ 0 & 0 & 0 & R\sqrt{1-\frac{r_o}{R}}\sin^2\theta \end{bmatrix}. \tag{C.5}$$

K can then be calculated:

$$\begin{aligned} K &= h^{\mu\nu}K_{\mu\nu} \\ &= -\frac{1}{(1-\frac{r_o}{r})}\frac{-\sqrt{1-\frac{r_o}{R}}r_o}{2R^2} + \frac{1}{R^2}R\sqrt{1-\frac{r_o}{R}} + \frac{1}{R^2\sin^2\theta}R\sqrt{1-\frac{r_o}{R}}\sin^2\theta \\ &= \frac{r_o}{2R^2\sqrt{1-\frac{r_o}{R}}} + \frac{1}{R}\sqrt{1-\frac{r_o}{R}} + \frac{1}{R}\sqrt{1-\frac{r_o}{R}} \\ &= \frac{r_o}{2R^2\sqrt{1-\frac{r_o}{R}}} + \frac{2}{R}\sqrt{1-\frac{r_o}{R}}. \end{aligned} \tag{C.6}$$

The next step consists of doing the same procedure in flat space, which corresponds to setting $r_o = 0$ so now $f(r) = 1$ and the metric is

$$ds^2 = -dt^2 + dr^2 + r^2 d\theta^2 + r^2\sin^2\theta d\phi^2. \tag{C.7}$$

Then taking the constant $r = R$ embedding

$$ds^2 = -dt^2 + r^2 d\theta^2 + r^2\sin^2\theta d\phi^2, \tag{C.8}$$

yields

$$\Gamma^r_{\mu\nu} = \begin{bmatrix} 0 & 0 & 0 & 0 \\ 0 & 0 & 0 & 0 \\ 0 & 0 & -R & 0 \\ 0 & 0 & 0 & -R\sin^2\theta \end{bmatrix}, \tag{C.9}$$

and

$$K^{(0)}_{\mu\nu} = \begin{bmatrix} 0 & 0 & 0 & 0 \\ 0 & 0 & 0 & 0 \\ 0 & 0 & R & 0 \\ 0 & 0 & 0 & R\sin^2\theta \end{bmatrix}. \tag{C.10}$$

We then find $K^{(0)}$

$$\begin{aligned} K^{(0)} &= h^{\mu\nu}K_{\mu\nu}, \\ &= 1*0+1*0+\frac{1}{R^2}*R+\frac{1}{R^2\sin^2\theta}R\sin^2\theta, \\ &= \frac{2}{R}. \end{aligned} \tag{C.11}$$

Now $T_{\mu\nu}$ can be worked out:

$$T_{\mu\nu} = -\frac{1}{8\pi}\left(K_{\mu\nu} - h_{\mu\nu}K - (K^{(0)}_{\mu\nu} - h_{\mu\nu}K^{(0)})\right). \tag{C.12}$$

We will show the explicit computation for the T_{tt} component

$$\begin{aligned} T_{tt} &= -\frac{1}{8\pi}\left(K_{tt} - h_{tt}K - (K^{(0)}_{tt} - h_{tt}K^{(0)})\right) \\ &= -\frac{1}{8\pi}\left(\frac{-\sqrt{1-\frac{r_o}{R}}r_o}{2R^2} + \left(1-\frac{r_o}{r}\right)\left(\frac{r_o}{2R^2\sqrt{1-\frac{r_o}{R}}} + \frac{2}{R}\sqrt{1-\frac{r_o}{R}}\right) + (-1+\frac{r_o}{R})\frac{2}{R}\right) \\ &= -\frac{1}{8\pi}\left(\frac{-\sqrt{1-\frac{r_o}{R}}r_o}{2R^2} + \frac{r_o\sqrt{1-\frac{r_o}{R}}}{2R^2} + \frac{2}{R}\left(1-\frac{r_o}{R}\right)^{\frac{3}{2}} - \frac{2}{R} + \frac{r_o}{R}\frac{2}{R}\right). \end{aligned} \tag{C.13}$$

Expanding this in $\frac{r_o}{R}$, we have

$$T_{tt} = \frac{1}{8\pi}\frac{r_o}{R^2}. \tag{C.14}$$

The rest of the components follow in a similar manner.

D Eddington–Finkelstein Coordinates

This section gives an example of switching to Eddington–Finkelstein coordinates [1] as follows:

$$\begin{aligned} &\sigma^a \to \sigma^a - u^a r_*, \qquad r_* = \int \frac{1}{f(r)} dr, \\ &d\sigma^a \to d\sigma^a - u^a \frac{1}{f(r)} dr. \end{aligned} \tag{D.1}$$

We use the example of a typical boosted black brane

$$ds^2 = (\eta_{ab} + u_a u_b (1 - f(r)))\, d\sigma^a d\sigma^b + \frac{1}{f(r)} dr^2 + r^2 d\Omega_2^2, \tag{D.2}$$

and apply the transformation

$$ds^2 = (\eta_{ab} + u_a u_b (1 - f(r))) \left(d\sigma^a - u^a \frac{dr}{f(r)} \right) \left(d\sigma^b - u^b \frac{dr}{f(r)} \right) + \frac{1}{f(r)} dr^2 r^2 d\Omega_{n+1}^2. \tag{D.3}$$

Expanding

$$\begin{aligned} ds^2 &= \eta_{ab} d\sigma^a d\sigma^b - \eta_{ab} u^a d\sigma^b \frac{dr}{f(r)} - \eta_{ab} u^b d\sigma^a \frac{dr}{f(r)} + \eta_{ab} u^a u^b \frac{dr^2}{f(r)^2} + \\ &u_a u_b (1 - f(r)) d\sigma^a d\sigma^b - u_a u_b (1 - f(r)) d\sigma^a u^b \frac{dr}{f(r)} - u_a u_b (1 - f(r)) d\sigma^b u^a \frac{dr}{f(r)} \\ &+ u_a u_b (1 - f(r)) u^a u^b \frac{dr^2}{f(r)^2} + \frac{1}{f(r)} dr^2 + r^2 d\Omega_{n+1}^2, \end{aligned} \tag{D.4}$$

and using

$$u_a u_b u^a u^b = u_a \eta^{ac} u_c u_b \eta^{bd} u_d = (-1)^2 = 1, \tag{D.5}$$

gives

$$\begin{aligned} ds^2 &= \eta_{ab}d\sigma^a d\sigma^b - 2u_c d\sigma^c \frac{dr}{f(r)} - \frac{dr^2}{f(r)^2} \\ &+u_a u_b(1-f(r))d\sigma^a d\sigma^b + 2u_c(1-f(r))d\sigma^c \frac{dr}{f(r)} + (1-f(r))\frac{dr^2}{f(r)^2} \\ &+\frac{1}{f(r)}dr^2 + r^2 d\Omega_{n+1}^2, \end{aligned} \tag{D.6}$$

which can be written as

$$ds^2 = P_{ab}d\sigma^a d\sigma^b - f(r)d\sigma^a d\sigma^b + 2u_c d\sigma^c + r^2 d\Omega_{n+1}^2, \tag{D.7}$$

where $P_{ab} = \eta_{ab} + u_a u_b$ is the orthogonal projector.

E MAE of Myers–Perry Black branes

In section 7, we used the method of matched asymptotic expansion to find the overlap region of the ultra-spinning Myers–Perry black hole, starting with the near region and then applying the asymptotic limit. It is worthwhile to examine whether the same metric is achieved if the opposite procedure is put into place, namely, if one takes the $r \gg r_o$ limit before taking the $a \gg r\cos\theta$ limit. This section deals with verifying that the resulting metric is indeed the same as previously obtained (7.10), up to second order. We also apply this procedure to the doubly-spinning case at ideal order.

E.1 Singly-Spinning Case

We start with (3.7) which is in terms of r_+ so this limit we take is $r \gg r_+$. The only terms affected by the limit are $\frac{\mu}{r^n\Sigma}$ and $\frac{\Sigma}{\Delta}$. Starting with (3.7) and putting the relevant terms in terms of $\frac{r_+}{r}$ gives:

$$\begin{aligned}
\mu &= \frac{r_+^n}{\cos^n\theta}\left(\frac{r_+^2}{\cos^2\theta}+a^2\right)\\
\frac{\mu}{r^n\Sigma} &= \frac{r_+^n\left(r_+^2+a^2\right)}{r^n\left(r^2+a^2\cos^2\theta\right)} \to \frac{r_+^n\left(\frac{r_+^2}{r^2}+\frac{a^2}{r^2}\right)}{r^n\left(1+\frac{a^2}{r^2}\cos^2\theta\right)}\\
\frac{\Sigma}{\Delta} &= \frac{r^2+a^2\cos^2\theta}{r^2+a^2-\frac{r_+^n}{r^n}\left(r_+^2+a^2\right)}dr^2 \to \frac{1+\frac{a^2}{r^2}\cos^2\theta}{1+\frac{a^2}{r^2}-\frac{r_+^n}{r^n}\left(\frac{r_+^2}{r^2}+\frac{a^2}{r^2}\right)}dr^2.
\end{aligned} \tag{E.1}$$

Expanding $\frac{\Sigma}{\Delta}$ up to second order in $\frac{r_+}{r}$ gives, for $n=1$[4]:

$$\frac{\Sigma}{\Delta} = \frac{1+\frac{a^2\cos^2\theta}{r^2}}{1+\frac{a^2}{r^2}} + \frac{\left(1+\frac{a^2\cos^2\theta}{r^2}\right)\frac{a^2r_+}{r^3}}{\left(1+\frac{a^2}{r^2}\right)^2} + \frac{\left(1+\frac{a^2\cos^2\theta}{r^2}\right)\frac{a^4r_+^2}{r^6}}{\left(1+\frac{a^2}{r^2}\right)^3}, \tag{E.2}$$

[4]When taking higher orders of $\frac{r_+^n}{r^n}$, the next order terms kept are $\frac{r_+^{2n}}{r^{2n}}$.

and for n=2:

$$\frac{\Sigma}{\Delta}=\frac{1+\frac{a^2\cos^2\theta}{r^2}}{1+\frac{a^2}{r^2}}+\frac{\left(1+\frac{a^2\cos^2\theta}{r^2}\right)\frac{a^2r_+^2}{r^5}}{\left(1+\frac{a^2}{r^2}\right)^2}+\frac{\left(1+\frac{a^2\cos^2\theta}{r^2}\right)\left(1+\frac{a^2}{r^2}+\frac{a^4}{r^4}\right)\frac{r_+^4}{r^4}}{\left(1+\frac{a^2}{r^2}\right)^3}. \tag{E.3}$$

Taking higher and higher n, a pattern emerges (This generalization works for $n\geq 2$ as when $n=1$, the $n+2$ term is third order):

$$\frac{\Sigma}{\Delta}=\frac{\left(1+\frac{a^2\cos^2\theta}{r^2}\right)}{\left(1+\frac{a^2}{r^2}\right)}+\frac{\left(1+\frac{a^2\cos^2\theta}{r^2}\right)\frac{a^2}{r^2}\frac{r_+^n}{r^n}}{\left(1+\frac{a^2}{r^2}\right)^2}+\frac{\left(1+\frac{a^2\cos^2\theta}{r^2}\right)\frac{r_+^{n+2}}{r^{n+2}}}{\left(1+\frac{a^2}{r^2}\right)^2}+\frac{\left(1+\frac{a^2\cos^2\theta}{r^2}\right)\frac{a^4}{r^4}\frac{r_+^{2n}}{r^{2n}}}{\left(1+\frac{a^2}{r^2}\right)^3}. \tag{E.4}$$

Taking $r_o=r_+\cos\theta$ and $r\cos\theta\to r$:

$$\begin{aligned}\frac{\Sigma}{\Delta}=\Bigg(&\frac{\left(1+\frac{a^2\cos^4\theta}{r^2}\right)}{\left(1+\frac{a^2\cos^2\theta}{r^2}\right)}+\frac{\left(1+\frac{a^2\cos^4\theta}{r^2}\right)\frac{a^2\cos^2\theta}{r^2}\frac{r_o^n}{r^n}}{\left(1+\frac{a^2\cos^2\theta}{r^2}\right)^2}+\\&\frac{\left(1+\frac{a^2\cos^4\theta}{r^2}\right)\frac{r_o^{n+2}}{r^{n+2}}}{\left(1+\frac{a^2\cos^2\theta}{r^2}\right)^2}+\frac{\left(1+\frac{a^2\cos^4\theta}{r^2}\right)\frac{a^4\cos^4\theta}{r^4}\frac{r_o^{2n}}{r^{2n}}}{\left(1+\frac{a^2\cos^2\theta}{r^2}\right)^3}\Bigg)\frac{dr^2}{\cos^2\theta}.\end{aligned} \tag{E.5}$$

For $\frac{\mu}{r^n\Sigma}$, when going up to second order, only the $n=1$ case has third order terms that must be truncated:

$$\frac{\mu}{r^n\Sigma}=\frac{r_+\left(\frac{r_+^2}{r^2}+\frac{a^2}{r^2}\right)}{r\left(1+\frac{a^2\cos^2\theta}{r^2}\right)}\to\frac{r_+\frac{a^2}{r^2}}{r\left(1+\frac{a^2}{r^2\cos^2\theta}\right)}=\frac{r_o\frac{a^2\cos^2\theta}{r^2}}{r\left(1+\frac{a^2}{r^2}\cos^4\theta\right)}. \tag{E.6}$$

Starting first with $n=1$, and later moving on to the general n case, the ultra-spinning limit is now taken. The terms affected by this expansion are $\frac{\Sigma}{\Delta}$, $\frac{\mu}{r^n\Sigma}$. The terms in front of $d\theta^2$ and $d\phi^2$ also have $r^2/a^2\cos^2\theta$ terms but they do not change as they are second order. After the asymptotic limit, taking $n=1$, these terms are:

$$\begin{aligned}\frac{\Sigma}{\Delta}&=\frac{\left(1+\frac{a^2\cos^4\theta}{r^2}\right)}{\left(1+\frac{a^2\cos^2\theta}{r^2}\right)}+\frac{\left(1+\frac{a^2\cos^4\theta}{r^2}\right)\frac{a^2\cos^2\theta}{r^2}\frac{r_o}{r}}{\left(1+\frac{a^2\cos^2\theta}{r^2}\right)^2}+\frac{\left(1+\frac{a^2\cos^4\theta}{r^2}\right)\frac{a^4\cos^4\theta}{r^4}\frac{r_o^2}{r^2}}{\left(1+\frac{a^2\cos^2\theta}{r^2}\right)^3},\\\frac{\mu}{r^n\Sigma}&=\frac{r_o\frac{a^2\cos^2\theta}{r^2}}{r\left(1+\frac{a^2}{r^2}\cos^4\theta\right)}.\end{aligned} \tag{E.7}$$

Taking the ultra-spinning limit $a\cos\theta \gg r$ up to second order turns these terms into:

$$\begin{aligned}\frac{\Sigma}{\Delta} &= \cos^2\theta\left(1+\frac{r_o}{r}+\frac{r_o^2}{r^2}\right)+\left(1+\frac{r_o}{r}+\frac{r_o^2}{r^2}-\cos^2\theta\left(1+2\frac{r_o}{r}+3\frac{r_o^2}{r^2}\right)\right)\frac{r^2}{a^2\cos^2\theta},\\ \frac{\mu}{r^n\Sigma} &= \frac{r_o}{r\cos^2\theta}-\frac{r_o}{r\cos^4\theta}\frac{r^2}{a^2\cos^2\theta}.\end{aligned} \tag{E.8}$$

Now looking at the general n case, starting with equation (E.5), $\frac{\Sigma}{\Delta}$ turns into:

$$\frac{\Sigma}{\Delta} = \cos^2\theta\left(1+\frac{r_o}{r}+\frac{r_o^2}{r^2}\right)+\left(1+\frac{r_o}{r}+\frac{r_o^2}{r^2}-\cos^2\theta\left(1+2\frac{r_o}{r}+3\frac{r_o^2}{r^2}+\frac{r_o^{n+2}}{r^{n+2}}\right)\right)\frac{r^2}{a^2\cos^2\theta}, \tag{E.9}$$

and $\frac{\mu}{r^n\Sigma}$ becomes

$$\frac{\mu}{r^n\Sigma} = \frac{r_o^n\left(\frac{r_o^2}{r^2}+\frac{a^2\cos^2\theta}{r^2}\right)}{r^n\left(1+\frac{a^2}{r^2}\cos^4\theta\right)} \to \frac{r_o^n}{r^n\cos^2\theta}+\frac{r_o^n\left(\frac{r_o^2}{r^2}\cos^2\theta-1\right)\frac{r^2}{a^2\cos^2\theta}}{r^n\cos^4\theta}. \tag{E.10}$$

To summarize, in general n dimensions:

$$\begin{aligned}\frac{\Sigma}{\Delta} &= \cos^2\theta\left(1+\frac{r_o}{r}+\frac{r_o^2}{r^2}\right)+\left(1+\frac{r_o}{r}+\frac{r_o^2}{r^2}-\cos^2\theta\left(1+2\frac{r_o}{r}+3\frac{r_o^2}{r^2}+\frac{r_o^{n+2}}{r^{n+2}}\Theta_{(n-2)}\right)\right)\frac{r^2}{a^2\cos^2\theta},\\ \frac{\mu}{r^n\Sigma} &= \frac{r_o^n}{r^n\cos^2\theta}+\frac{r_o^n\left(\frac{r_o^2\cos^2\theta}{r^2}\Theta_{(n-2)}-1\right)\frac{r^2}{a^2\cos^2\theta}}{r^n\cos^4\theta},\end{aligned} \tag{E.11}$$

where Θ is the step function. The ideal limit (with orders of $\frac{r_o^n}{r^n}$ and $\left(\frac{r}{a\cos\theta}\right)^0$) is taken in order to compare with equation (7.10), giving:

$$\begin{aligned}ds^2 = &-dt^2+\frac{r_o^n}{r^n\cos^2\theta}(dt-a\sin^2\theta d\phi)^2+\left(1+\frac{r_o^n}{r^n}\right)dr^2\\ &+a^2\cos^2\theta d\theta^2+a^2\sin^2\theta d\phi^2+r^2\cos^2\theta d\Omega_{n+1}^2,\end{aligned} \tag{E.12}$$

which, after making the appropriate changes of variables, matches (7.10).

E.2 Doubly-Spinning Case

Now we apply this procedure to the doubly-spinning case, starting with the metric (3.9). In [6], it was found that taking the ultra-spinning limit turns this metric into

$$\begin{aligned} ds^2 &= -dt^2 + d\rho^2 + dz^2 + \frac{r_o^n}{\Sigma r^{n-2}}\Big(\frac{dt}{\cos\theta_*} - tan\theta_* dz - b\sin^2\psi d\phi\Big)^2 + \frac{\Sigma}{\Delta}dr^2 + \Sigma d\psi^2 \\ &\quad + \left(r^2+b^2\right)\sin^2\psi d\phi^2 + r^2\cos^2\psi d\phi^2 + r^2\cos^2\psi d\Omega_{n-1}^2, \\ \Sigma &= r^2 + b^2\cos^2\psi, \qquad \Delta = r^2 + b^2 - \frac{r_o^n}{r^{n-2}}, \end{aligned} \tag{E.13}$$

where the following transformations have been made

$$\begin{aligned} &r\cos\theta_* \to r, \qquad r_+\cos\theta_* \to r_o, \qquad b \to b\cos\theta_*, \\ &\rho = a\sin\theta, \qquad z = \rho_*\phi_1, \qquad \phi_2 \to \phi. \end{aligned} \tag{E.14}$$

We take the $r \gg r_o$ limit where the only term affected is the dr^2 term:

$$\frac{\Sigma}{\Delta}dr^2 \to \frac{r^2 + b^2\cos^2\psi}{r^2+b^2}\left(1 + \frac{r_o^n}{r^{n-2}}\frac{1}{r^2+b^2}\right)dr^2. \tag{E.15}$$

Now we do the opposite procedure, taking the asymptotic limit first. We start by writing μ in terms of r_+:

$$\mu = r_+^{n+2}\left(1+\frac{a^2}{r_+^2}\right)\left(1+\frac{b^2}{r_+^2}\right) = r_+^{n+2}\left(1+\frac{a^2}{r_+^2}\right)B, \tag{E.16}$$

with the renaming $a_1 = a$ and $a_2 = b$, and B=$\left(1+\frac{b^2}{r_+^2}\right)$. Applying the asymptotic limit to the dr^2 term, we get

$$\frac{\Pi F}{\Pi - \frac{\mu}{r^{n+2}}}dr^2 \to F\left(1 + \frac{r_+^{n+2}}{r^{n+2}}\frac{\left(1+\frac{a^2}{r_+^2}\right)B}{\Pi}\right)dr^2, \tag{E.17}$$

and outside the squared term we get

$$\frac{\mu}{r^{n+2}\Pi F} \to \frac{r_+^{n+2}\left(1+\frac{a^2}{r_+^2}\right)B}{r^{n+2}\Pi F}. \tag{E.18}$$

As these are the only terms containing r_+, everything else remains the same. Now we can again take the ultra-spinning limit, with $a\cos\theta \gg r$, $a\cos\theta \gg r_+$ and $a \gg b$. The terms outside dr^2 become

$$\left(\cos^2\theta - \frac{b^2\cos^2\theta\sin^2\psi}{r^2+b^2}\right)\left(1+\frac{r_+^n}{r^n}\frac{B}{1+\frac{b^2}{r^2}}\right)dr^2. \tag{E.19}$$

Making the changes $r_o^n = r_+^n\cos^n\theta B$, $r\cos\theta \to r$, and $b\cos\theta \to b$:

$$\left(\frac{r^2+b^2\cos^2\psi}{r^2+b^2}\right)\left(1+\frac{r_o^n}{r^{n-2}}\frac{1}{r^2+b^2}\right)dr^2, \tag{E.20}$$

and outside the squared term:

$$\frac{r_o^n}{r^{n-2}}\left(\frac{1}{r^2+b^2\cos^2\psi}\right), \tag{E.21}$$

which matches what we found before.

F Explicit Large Functions

In this section is where the large functions of this thesis are stored.

Doubly-Spinning Black Ring

The functions in the black string solution with two angular momenta (3.27) are

$$\begin{aligned}
\Omega =& -\frac{2k\lambda\sqrt{(1+\nu)^2-\lambda^2}}{H(y,x)}\Big[(1-x^2)y\sqrt{\nu}d\phi \\
&+\frac{1+y}{1-\lambda+\nu}(1+\lambda-\nu+x^2y\nu(1-\lambda-\nu)+2\nu x(1-y))d\psi\Big], \\
G(x) =& (1-x^2)(1+\lambda x+\nu x^2), \\
H(x,y) =& 1+\lambda^2-\nu^2+2\lambda\nu(1-x^2)y+2x\lambda(1-y^2\nu^2)+x^2y^2\nu(1-\lambda^2-\nu^2), \\
J(x,y) =& \frac{2k^2(1-x^2)(1-y^2)\lambda\sqrt{\nu}}{(x-y)(1-\nu)^2}\left(1+\lambda^2-\nu^2+2(x+y)\lambda\nu-xy\nu(1-\lambda^2-\nu^2)\right), \\
F(x,y) =& \frac{2k^2}{(x-y)^2(1-\nu)^2}\Big[G(x)(1-y^2)\Big[\left((1-\nu^2)-\lambda^2\right)(1+\nu) \\
&+y\lambda(1-\lambda^2+2\nu-3\nu^2)\Big]+G(y)[2\lambda^2+x\lambda((1-\nu)^2+\lambda^2) \\
&+x^2((1-\nu)^2-\lambda^2)(1+\nu)+x^3\lambda(1-\lambda^2-3\nu^2+2\nu^3)-x^4(1-\nu)\nu(-1+\lambda^2+\nu^2)]\Big].
\end{aligned} \tag{F.1}$$

AdS/Fluid metric Functions

The metric functions are given by a perturbative expansion:

$$\begin{aligned}
S(r,x) =& 1-\sum_{k=1}^{\infty}\epsilon^k s_a^{(k)}, \\
\chi_{\mu\nu}(r,x) =& -r^2 f(br)u_\mu u_\nu + r^2 P_{\mu\nu} \\
&+\sum_{k=1}^{\infty}\epsilon^k\left(s_c^{(k)}r^2P_{\mu\nu}+s_b^{(k)}u_\mu u_\nu+j_\nu^{(k)}u_\mu+j_\mu^{(k)}u_\nu+t_{\mu\nu}^{(k)}\right), \\
f(y) =& \frac{1}{1-\frac{1}{y^4}},
\end{aligned} \tag{F.2}$$

where the functions $(s_a^{(k)}, s_b^{(k)}...)$ are local functions of the inverse temperature $b(x)$. Ond one can consider them arbitrary functions of r and x^μ for this thesis, the same goes for $j_\mu^{(k)}$ and $t_{\mu\nu}^{(k)}$.

Weyl Covariant Form of AdS/Fluid metric

The functions in the Weyl covariant form of the metric (6.34) are

$$\begin{aligned}\mathcal{B} =& rA_\mu - \mathcal{S}_{\mu\lambda}u^\lambda - v_1(br)P_\mu^\nu D_\lambda \sigma_\nu^\lambda \\ &+u_\mu\left[\frac{1}{2}r^2 f(br) + \frac{1}{4}\left(1-f(br)\right)\omega_{\alpha\beta}\omega^{\alpha\beta} + \mathbf{v}_2(br)\frac{\sigma_{\alpha\beta}\sigma^{\alpha\beta}}{d-1}\right], \end{aligned} \tag{F.3}$$

$$\begin{aligned}\mathcal{G} =& r^2 P_{\mu\nu} - \omega_\mu^\lambda \omega_{\lambda\nu} + 2(br)^2 \mathbf{g}_1(br)\left[\frac{1}{b}\sigma_{\mu\nu} + \mathbf{g}_1(br)\sigma_\mu^\lambda \sigma_{\lambda\nu}\right] - \mathbf{g}_2(br)\frac{\sigma_{\alpha\beta}\sigma^{\sigma\beta}}{d-1}P_{\mu\nu} \end{aligned} \tag{F.4}$$

$$- \mathbf{g}_3(br)[\mathcal{J}_{1\mu\nu} + \frac{1}{2}\mathcal{J}_{3\mu\nu} + 2\mathcal{J}_{2\mu\nu}] + \mathbf{g}_4(br)[\mathcal{J}_{1\mu\nu} + \mathcal{J}_{4\mu\nu}], \tag{F.5}$$

where $\mathcal{J}_i^{\mu\nu}$'s are the set of symmetric traceless tensors which transform homogeneously under Weyl rescalings

$$\begin{aligned}\mathcal{J}_1^{\mu\nu} &= 2\mu^\alpha \mathcal{D}_\alpha \sigma^{\mu\nu}, \\ \mathcal{J}_2^{\mu\nu} &= C^{\mu\ \nu}_{\alpha\ \beta}\, u^\alpha u^\beta, \\ \mathcal{J}_3^{\mu\nu} &= 4\sigma^{\alpha\langle\mu}\sigma_\alpha^{\nu\rangle}, \\ \mathcal{J}_4^{\mu\nu} &= 4\sigma^{\alpha\langle\mu}\omega_\alpha^{\nu\rangle}, \\ \mathcal{J}_5^{\mu\nu} &= \omega^{\alpha\langle\mu}\omega_\alpha^{\nu\rangle}, \end{aligned} \tag{F.6}$$

and functions are

$$
\begin{aligned}
\mathbf{g}_1(y) &= \int_y^\infty d\zeta \frac{\zeta^{d-1}-1}{\zeta(\zeta^d-1)}, \\
\mathbf{g}_2(y) &= 2y^2 \int_y^\infty \frac{d\xi}{\xi^2} \int_\xi^\infty d\zeta\, \zeta^2 \mathbf{g}_1'(\zeta)^2, \\
\mathbf{g}_3(y) &= y^2 \int_y^\infty d\xi \frac{\xi^{d-2}-1}{\xi(\xi^d-1)}, \\
\mathbf{g}_4(y) &= y^2 \int_y^\infty \frac{d\xi}{\xi(\xi^d-1)} \int_1^\xi d\zeta\, \zeta^{d-3} \Big(1+(d-1)\zeta \mathbf{g}_1(\zeta) + 2\zeta^2 \mathbf{g}_1'(\zeta)\Big), \\
\mathbf{v}_1(y) &= \frac{2}{y^{d-2}} \int_y^\infty d\xi\, \xi^{d-1} \int_\xi^\infty d\zeta \frac{\zeta-1}{\zeta^3(\zeta^d-1)}, \\
\mathbf{v}_2(y) &= \frac{1}{2y^{d-2}} \int_y^\infty \frac{d\xi}{\xi^2} \Big[1 - \xi(\xi-1)\mathbf{g}_1'(\xi) - 2(d-1)\xi^{d-1} \\
&\quad + \big(2(d-1)\xi^d - (d-2)\big) \int_\xi^\infty d\zeta\, \zeta^2 \mathbf{g}_1'(\zeta)^2 \Big].
\end{aligned}
\tag{F.7}
$$

$C_{\mu\nu\lambda\sigma}$ is the Weyl tensor, the trace free part of the Riemann tensor, which in $d \geq 3$ is

$$
C_{\mu\nu\lambda\sigma} \equiv R_{\mu\nu\lambda\sigma} + 4\delta^\alpha_{[\mu} g_{\nu][\lambda} \delta^\beta_{\sigma]} \mathcal{S}_{\alpha\beta}, \tag{F.8}
$$

and $\mathcal{S}_{\mu\nu}$ is the Schouten tensor

$$
\mathcal{S}\mu\nu = \frac{1}{d-2} \left(R_{\mu\nu} - \frac{R g_{\mu\nu}}{2(d-1)} \right). \tag{F.9}
$$

Functions for Second Order Energy-Momentum Tensor

The functions to find $\tilde{\tau}_\omega$ in the second order energy-momentum tensor are:

$$
\begin{aligned}
F(br) &= \int_{br}^\infty \frac{y^{d-1}-1}{y(y^d-1)} dy, \\
H_2(br) &= \frac{1}{2} F(br)^2 - \int_{br}^\infty \frac{d\xi}{\xi(\xi^d-1)} \int_1^\xi \frac{y^{d-2}-1}{y(y^d-1)} dy.
\end{aligned}
\tag{F.10}
$$

Gregory–Laflamme Instability Differential Equation

The differential equation to find the Gregory–Laflamme instability of a string is

$$
\begin{aligned}
0 =& \Big[-\Omega^2 - \mu^2 V + \frac{(\mathtt{d}-3)^2 \left(\frac{r_+}{r}\right)^{2(\mathtt{d}-3)}}{4r^2} \Big] H^{tr\,\prime\prime} - \left[\mu^2 \left[(\mathtt{d}-2) - 2\left(\frac{r_+}{r}\right)^{\mathtt{d}-3} + (4-\mathtt{d}) \left(\frac{r_+}{r}\right)^{2(\mathtt{d}-3)} \right] \right. \\
&+ \frac{\Omega^2 [(\mathtt{d}-2) + (2\mathtt{d}-7)\left(\frac{r_+}{r}\right)^{\mathtt{d}-3}]}{rV} + \frac{1}{4r^3 V} 3(\mathtt{d}-3)^2 \left(\frac{r_+}{r}\right)^{2(\mathtt{d}-3)} [(\mathtt{d}-2) - \left(\frac{r_+}{r}\right)^{\mathtt{d}-3}] \Big] H^{tr\,\prime} \\
&+ \left[\left(\mu^2 + \Omega^2/V\right)^2 + \frac{1}{4r^2 V^2} \Omega^2 \left[4(\mathtt{d}-2) - 8(\mathtt{d}-2)\left(\frac{r_+}{r}\right)^{\mathtt{d}-3} - (53 - 34\mathtt{d} + 5\mathtt{d}^2) \left(\frac{r_+}{r}\right)^{2(\mathtt{d}-3)} \right] \right. \\
&+ \frac{1}{4r^2 V} \mu^2 \left[4(\mathtt{d}-2) - 4(3\mathtt{d}-7)\left(\frac{r_+}{r}\right)^{\mathtt{d}-3} + (\mathtt{d}^2 + 2\mathtt{d} - 11)\left(\frac{r_+}{r}\right)^{2(\mathtt{d}-3)} \right] \\
&\left. + \frac{1}{4r^4 V^2} (\mathtt{d}-3)^2 \left(\frac{r_+}{r}\right)^{2(\mathtt{d}-3)} \left[(\mathtt{d}-2)(2\mathtt{d}-5) - (\mathtt{d}-1)(\mathtt{d}-2)\left(\frac{r_+}{r}\right)^{\mathtt{d}-3} + \left(\frac{r_+}{r}\right)^{2(\mathtt{d}-3)} \right] \right] H^{tr}. \qquad \text{(F.11)}
\end{aligned}
$$

References

[1] J. Camps, R. Emparan, and N. Haddad, "Black brane viscosity and the Gregory-Laflamme instability," *Journal of High Energy Physics*, vol. 2010, no. 5, 2010, ISSN: 10298479. DOI: 10.1007/JHEP05(2010)042. arXiv: 1003.3636.

[2] J. Camps and R. Emparan, "Derivation of the blackfold effective theory," *Journal of High Energy Physics*, vol. 2012, no. 3, 2012, ISSN: 11266708. DOI: 10.1007/JHEP03(2012)038. arXiv: 1201.3506.

[3] M. M. Caldarelli, J. Camps, B. Goutéraux, and K. Skenderis, "AdS/Ricci-flat correspondence," *Journal of High Energy Physics*, vol. 2014, no. 4, 2014, ISSN: 10298479. DOI: 10.1007/JHEP04(2014)071. arXiv: 1312.7874.

[4] S. M. Carroll, *Lecture notes on general relativity*, 1997. arXiv: gr-qc/9712019 [gr-qc].

[5] R. Emparan, T. Harmark, V. Niarchos, and N. A. Obers, "Essentials of blackfold dynamics," *Journal of High Energy Physics*, vol. 2010, no. 3, 2010, ISSN: 11266708. DOI: 10.1007/JHEP03(2010)063. arXiv: arXiv:0910.1601v2.

[6] J. Armas, J. Camps, T. Harmark, and N. A. Obers, "The Young modulus of black strings and the fine structure of blackfolds," *Journal of High Energy Physics*, vol. 2012, no. 2, 2012, ISSN: 11266708. DOI: 10.1007/JHEP02(2012)110. arXiv: arXiv:1110.4835v2.

[7] G. Oas. (2012). Full derivation of the schwarzschild solution, [Online]. Available: https://web.stanford.edu/~oas/SI/SRGR/notes/SchwarzschildSolution.pdf.

[8] S. Hollands and A. Ishibashi, "Black hole uniqueness theorems in higher dimensional spacetimes," *Classical and Quantum Gravity*, vol. 29, no. 16, pp. 1–67, 2012, ISSN: 02649381. DOI: 10.1088/0264-9381/29/16/163001. arXiv: 1206.1164.

[9] R. Emparan and H. S. Reall, "Black holes in higher dimensions," *Living Reviews in Relativity*, vol. 11, no. 1, Sep. 2008, ISSN: 1433-8351. DOI: 10.12942/lrr-2008-6. [Online]. Available: http://dx.doi.org/10.12942/lrr-2008-6.

[10] M. Heusler, "No hair theorems and black holes with hair," *Helv. Phys. Acta*, vol. 69, no. 4, N. Straumann, P. Jetzer, and G. V. Lavrelashvili, Eds., pp. 501–528, 1996. arXiv: gr-qc/9610019.

[11] (2016). General theorems about higher dimensional black holes, University of Leipzig, [Online]. Available: https://home.uni-leipzig.de/tet/?page_id=786.

[12] R. Emparan and H. S. Reall, "Black Rings," *Class. Quant. Grav.*, vol. 23, R169, 2006. DOI: 10.1088/0264-9381/23/20/R01. arXiv: hep-th/0608012.

[13] R. Emparan, T. Harmark, V. Niarchos, and N. A. Obers, "World-volume effective theory for higher-dimensional black holes," *Physical Review Letters*, vol. 102, no. 19, pp. 1–11, 2009, ISSN: 10797114. DOI: 10.1103/PhysRevLett.102.191301. arXiv: 0902.0427.

[14] R. Emparan, T. Harmark, V. Niarchos, N. A. Obers, and M. J. Rodríguez, "The phase structure of higher-dimensional black rings and black holes," *Journal of High Energy Physics*, vol. 2007, no. 10, 2007, ISSN: 11266708. DOI: 10.1088/1126-6708/2007/10/110. arXiv: arXiv:0708.2181v3.

[15] R. Emparan, "Blackfolds," *Black Holes in Higher Dimensions*, vol. 9781107013452, pp. 180–212, 2012. DOI: 10.1017/CBO9781139004176.009. arXiv: 1106.2021.

[16] R. C. Myers, "Myers–Perry black holes," *Black Holes in Higher Dimensions*, vol. 9781107013452, pp. 101–133, 2012. DOI: 10.1017/CBO9781139004176.006. arXiv: 1111.1903.

[17] C. M. Hirata. (2011). Stress-energy tensor and conservation of energy and momentum, California Institute of Technology, [Online]. Available: http://www.tapir.caltech.edu/~chirata/ph236/lec04.pdf.

[18] H. Reall. (2012). General relativity, University of Cambridge, [Online]. Available: https://www.damtp.cam.ac.uk/user/hsr1000/lecturenotes_2012.pdf.

[19] J. Brown and J. York James W., "Quasilocal energy and conserved charges derived from the gravitational action," *Phys. Rev. D*, vol. 47, pp. 1407–1419, 1993. DOI: 10.1103/PhysRevD.47.1407. arXiv: gr-qc/9209012.

[20] S. Bhattacharyya, S. Minwalla, V. E. Hubeny, and M. Rangamani, "Nonlinear fluid dynamics from gravity," *Journal of High Energy Physics*, vol. 2008, no. 2, 2008, ISSN: 11266708. DOI: 10.1088/1126-6708/2008/02/045. arXiv: 0712.2456.

[21] M. Rangamani, "Gravity and hydrodynamics: Lectures on the fluid-gravity correspondence," *Classical and Quantum Gravity*, vol. 26, no. 22, 2009, ISSN: 02649381. DOI: 10.1088/0264-9381/26/22/224003. arXiv: 0905.4352.

[22] Z. Z. Ma, "The Bekenstein-Hawking entropy of higher-dimensional rotating black holes," *Prog. Theor. Phys.*, vol. 115, pp. 863–871, 2006. DOI: 10.1143/PTP.115.863. arXiv: hep-th/0512130.

[23] R. Gregory and R. Laflamme, "Black strings and p-branes are unstable," *Phys. Rev. Lett.*, vol. 70, pp. 2837–2840, 1993. DOI: 10.1103/PhysRevLett.70.2837. arXiv: hep-th/9301052.

[24] R. Gregory, "The gregory–laflamme instability," *Black Holes in Higher Dimensions*, vol. 9781107013452, pp. 29–43, 2012. DOI: 10.1017/CBO9781139004176.003. arXiv: 1107.5821.

[25] P. Figueras, M. Kunesch, and S. Tunyasuvunakool, "End Point of Black Ring Instabilities and the Weak Cosmic Censorship Conjecture," *Physical Review Letters*, vol. 116, no. 7, 2016, ISSN: 10797114. DOI: 10.1103/PhysRevLett.116.071102. arXiv: 1512.04532.

[26] P. Figueras, M. Kunesch, and S. Tunyasuvunakool. (2016). Very thin black ring - gregory-laflamme instability, Youtube, [Online]. Available: https://www.youtube.com/watch?v=hBvaHLhlhE4.

[27] M. Headrick, *Differential geometry*, Brandeis University, Jul. 2015. [Online]. Available: http://people.brandeis.edu/~headrick/Mathematica/diffgeo.m.

[28] D. E. Vincent. (2014). Isotropic coordinates, University of Winnipeg, [Online]. Available: http://ion.uwinnipeg.ca/~vincent/4500.6-001/Cosmology/IsotropicCoordinates.htm.